Bulletin of Geophysics and Oceanography Vol. 65, n. 3, pp. 347-376; September 2024
DOI 10.4430/bgo00446

2D sharp boundary inversion to determine tectonic and geological features of geothermal fields through the magnetotelluric method: case study of the Mahallat reservoir in Iran

S.H. Hosseini[1], B. Oskooi[1,2], S. Ghanbarifar[1], S.M. Ghiasi[1], M. Abedi[3] and M.Y. Smirnov[2]

[1] *Institute of Geophysics, University of Tehran, Tehran, Iran*
[2] *Division of Geosciences and Environmental Engineering, Department of Civil, Environment and Natural Resources Engineering, University of Technology, Luleå, Sweden*
[3] *School of Mining Engineering, College of Engineering, University of Tehran, Tehran, Iran*

(Received: 22 July 2023; accepted: 30 November 2023; published online: 27 February 2024)

ABSTRACT Multiple processing approaches were applied to magnetotelluric data from the Mahallat geothermal field in central Iran to evaluate the dimensionality and geoelectric strike of the subterranean structures, as well as to comprehend the overall geometry of the targeted reservoir. While conventional smooth inversion methods can generate reliable models, their application, in the absence of initial information, may lead to unrealistic outcomes, especially in media with sharp resistivity contrasts. Consequently, a conventional smooth inversion, alongside the sharp boundary inversion techniques, is applied on real data through two profiles in order to investigate and compare the subsurface structural features. Ultimately, by adopting a target-oriented modelling approach, this study utilises the sharp boundary method to deduce a more suitable configuration for the characteristics of the geothermal reservoir. Thus, to a large extent, this approach can facilitate the interpretational complications of underground geothermal structures. Correspondingly, this research led to recognising a hydrothermal reservoir with a proper layout at a depth of 1,800 and 1,200 m underneath profiles A and B, respectively. Moreover, deeper reservoirs were identified and depicted as conceptual geological models obtained through the incorporation of sharp boundary inversion results and geological information.

Key words: magnetotelluric, Mahallat geothermal region, 2D sharp boundary inversion.

1. Introduction

Geothermal fields all around the world are limitless sources of thermal energy. This form of energy is conveyed to the surface through two primary mechanisms: volcanic eruptions or liquid circulation within a geothermal complex. Accordingly, hot springs are the surficial demonstration of hydrothermal circulation from a geothermal system, so that heated liquids rise through impenetrable rocks. Prior studies in the Mahallat region of central Iran indicate that the heat of the springs is due to the cooling process of the subsurface molten magma (Oskooi *et al*., 2013, 2016; Oskooi and Darijani, 2014; Ardestani *et al*., 2021; Hosseini *et al*., 2021; Talebi *et al*., 2023). Indeed, deep structural and geological events, such as faults, can cause the occurrence of hot springs. Notably, the karst phenomenon may also form hot springs. In such type of hot springs,

underground water resources are essential for transmitting the heat through the permeable karst rocks (Li *et al*., 2007, 2023; Tian *et al*., 2021). Geothermal energy has been known to be an essential energy source in Iran since the beginning of the 20th century (Noorollahi *et al*., 2009, 2019; Yousefi *et al*., 2010; Najafi and Ghobadian, 2011). The country holds vast hydrothermal systems (at least 14 explored geothermal zones) including over 50 active geothermal reservoirs in different areas (Dashti and Gholami Korzani, 2021; Noorollahi *et al*., 2019). Geothermal fields closely align with vast volcanic belts and tectonic activities. In this regard, the Mahallat geothermal field is one of the eminent geothermal regions in Iran (SUNA, 1998). Paramount geological complications, such as numerous hot springs, intrusive granites, granodiorite bodies within the sedimentary bed, and considerable surficial alterations, substantiate the existence of a geothermal system beneath the study area (Yazdi *et al*., 2016). Positioned within the tectonic framework of the Iranian plateau, the Mahallat field lies in the volcanic zone of central Iran. This zone has always been one of the active and dynamic regions during the different geological epochs (Alavi, 1994; Hassanzadeh and Wernicke, 2016). The western border of the study area is limited to the Sanandaj-Sirjan metamorphic zone.

Furthermore, central Iran is delimited by the Alborz and Makran zones at the northern and southern boundaries, respectively (Navai, 1976; Berberian, 1981; Ghorbani, 2013). In the central Iranian zone, where the Mahallat geothermal field is situated, a juxtaposition of the oldest metamorphic rocks (Precambrian) to the most recent active and semi-active volcanos can be observed (Ghorbani, 2021). Tectonic activities over the past geological periods have generated many faults in the region. The main fault, referred to as the Mahallat Fault and approximately 50 km long, passes through the north of Mahallat city, with an E-W orientation. In the continuation, this fault changes orientation to NE-SW and N-S. Some small-scale faults, apparently splits of the major fault, are also observed at the boundary of the formation units. Based on findings from previous geological and geochemical investigations, the major flow of the hydrothermal fluid is referred to be under the N-S faults (Porkhial *et al*., 2013).

There are various geophysical methods to characterise geothermal zones; however, the magnetotelluric (MT) approach would be an optimal choice for modelling the underground conductive and resistive layers. This is due to the significant changes that occur within the background resistivity of subsurface structures in geothermal fields, caused by high alteration levels. The advantage of the above method in examining geothermal regions is the sensitivity to the relevant index zones, such as the conductive caps or heat sources (Oskooi *et al*., 2012; Gingarimbun *et al*., 2017; Peng *et al*., 2019).

This study aims to obtain precise models from the MT data corresponding to the well-recognised geothermal zone of Mahallat. As is known, the ultimate goal of surveying geothermal zones is to identify the physical features of the area and, consequently, determine the main characteristics of the geothermal system components, such as reservoir, cap rock, heat source, and bedrock. Therefore, inverse modelling approaches are schemes of utmost importance to attain such objectives. Many studies have been conducted in the Mahallat geothermal area (Moghaddam *et al*., 2012; Nouraliee *et al*., 2015; Oskooi *et al*., 2016; Shirani *et al*., 2020; Ardestani *et al*., 2021). Hosseini *et al*. (2021) utilised magnetometry and MT surveys to study the geothermal zone. As a result, they proposed a heat source comprising intrusive igneous rocks at a depth from 3 to 4 km, along with a sandstone and shale reservoir with a depth ranging from approximately 300 to 2,300 m. This reservoir is affected by two faults and is capped by a travertine layer with a thickness of approximately 100 to 200 m. In previous studies in the area, the results also determined the depth of 100 m for shallow conductive cap rock with variable thickness relating to surface water penetration, and the depth of 1 to 3 km was also

proposed for the reservoir (Oskooi *et al*., 2013). It should be noted that the depth of 0.8 to 2 km, corresponding to the geothermal reservoir in the area, was recommended by utilising MT data and a conceptual model in the previous research (Oskooi *et al*., 2014).

In short, this research uses the two methods of smooth and sharp boundary inversion schemes, on a well-known geothermal field, to draw a correct analogy and distinguish the physical and geological properties of the subsurface structures (Smith *et al*., 1999; Rodi *et al*., 2001; DeGroot-Hedlin and Constable, 2004; Munoz *et al*., 2010; McGary *et al*., 2014). In fact, the study set out to investigate the impact of sharp boundary inversion schemes in achieving more useful information on geothermal targets. In cases of interpretation with prior information, a fairly valid strategy may be to set previously achieved constraints within the inverse modelling process. Hence, in this research, previously conducted studies, along with the currently performed smooth inversion, can lead towards a correctly finalised geophysical and geological conceptual model. In this research, both smooth and sharp boundary techniques are employed as complementary tools for interpretational proposes (Smith *et al*., 1999; Rodi *et al*., 2001). Notably, in exploration geophysics analyses, acquiring accurate edge perimeters of target anomalies for further investigations and modelling are considered fundamental issues for geophysicists and geological interpreters (Ghiasi *et al*., 2023). Deploying various techniques helps to suppress the intrinsic ambiguity arising from data interpretation. Therefore, separate investigations and comparisons of smooth and sharp boundary inversion methods were conducted on a synthetic model. The synthetic model enables specifying the strengths and weaknesses of the smooth and sharp boundary models through a controlled medium. By consolidating a variety of inversion methods, the interpreter would be able to achieve more accommodated models for realistic and concrete situations, especially in geothermal surveys with sharp contrasts of physical properties such as conductivity within subsurface structures. In this regard, the two methods are applied to Mahallat MT data. Fig. 1 illustrates the tree diagram of the research progression, which presents the detailed framework of the investigated scheme.

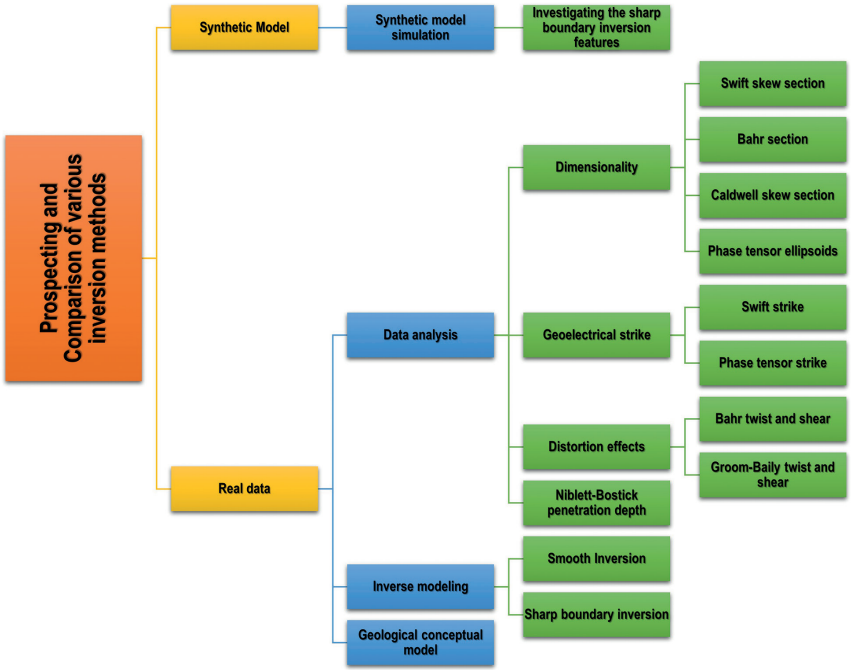

Fig. 1 - Tree diagram of the research procedure.

2. Geological settings

The Mahallat geothermal field is located in the volcanic zone of central Iran. One of the active zones during various geological eras, it is comparable to a triangle in the centre of Iran (Gansser, 1955; Alavi, 1994). Formed after the collision of the Arabian and Iranian plates, the central Iranian zone is bounded by the Alborz zone to the north and by the Makran zone to the south (Fig. 2). Large significant faults occur in and around the zone creating several blocks (McKenzie, 1972; Jackson *et al*., 2002; Ritz *et al*., 2006).

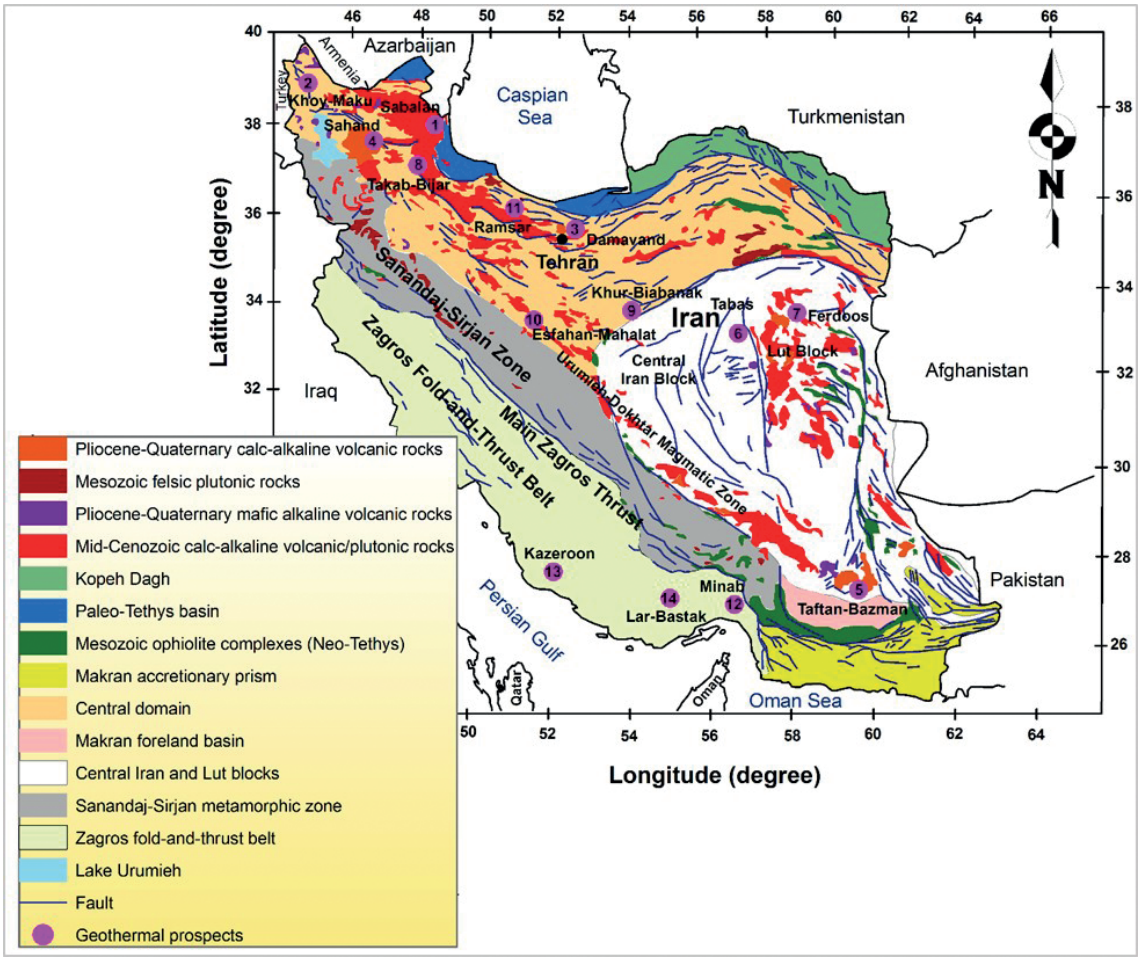

Fig. 2 - Simplified geological map of Iran including structural divisions. Known geothermal prospects are marked.

As shown in Fig. 2, there are almost 14 geothermal prospect regions in Iran, and the study area, within the central domain of the Iranian plate, is indicated as number 10.

Fig. 3 illustrates MT sites projected on the geological map of the Mahallat geothermal zone and shows the faults, formations, and topography. According to the map, the lithological units belong to the Palaeozoic, Mesozoic, and Cenozoic eras (Araghi, 2009). Magmatic activity in the area commenced from the Eocene era, within a sequence of Mesozoic and Palaeozoic sediments.

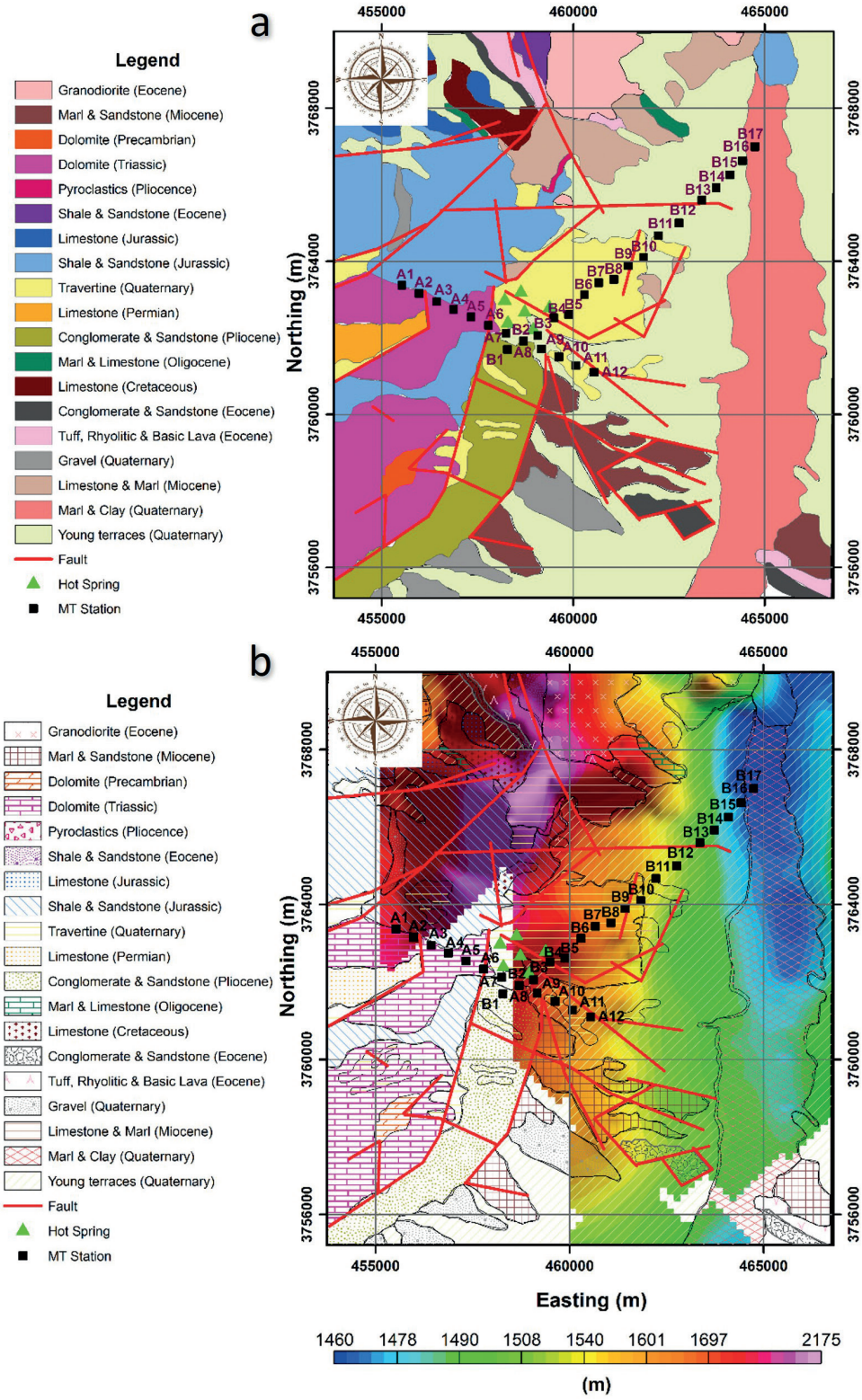

Fig. 3 - Detailed geological description of Mahallat geothermal region (a) and topography relief overlaid by the geological units (b). Two MT profiles over the studied geothermal reservoir are superimposed on the maps.

In terms of magmatic thermal activity investigations, the above-mentioned rocks underwent alteration due to a primary Miocene monzonitic batholith extending NW-SE. In conformity with the fractured limestone and dolomite units, the area provides appropriate permeability; thus, in some areas, where the clay caps prevent water from penetrating to the surface (hot water springs), the faults and fractures are capable of enhancing the permeability parameters. Some alluvial units are also present in the area, and the first-era lithology units belong to the Cambrian and Permian eras. The Cambrian era encompasses the Soltanieh, Zaygun, Lalun, and Mila formations. The Permian era includes limestone and dolomitic units, while other surficial lithologies, such as Triassic limestones and Eocene conglomerates, are located on southern heights. The Eocene sedimentary layers in the study area consist of conglomerates and igneous rocks; the conglomerate rocks are mainly exposed as rough plains with conglomerate and sandstone lithologies covering shales. The igneous units include surface chilled igneous rocks such as granite, granodiorite, andesite and basalt. In contrast, the granite rocks belong to the late Eocene-Oligocene epoch, the granodiorites to the Miocene, and andesite and basalts to the Eocene era. It is notable that the Jurassic epoch in the area involves the Shemshak formation, which contains grey shales and sandstones (Aghanabati, 2004).

The lithology of the area also consists of travertines associated with the fourth era and the Cretaceous limestones. Qom and Red-Upper formations are the most prominent in the study area, comprising Oligocene-Miocene limestone and marl, and red marl and Miocene conglomerates, respectively. In addition, numerous travertines are present and different geological alterations can also be observed within the area. Most of the alterations are the argillitisation-sericitisation types; however, some further alterations, such as the kaolinisation-alunitisation types, are also present in the area (Oskooi *et al*., 2013, 2016; Oskooi and Darijani, 2014). Geological alterations are closely related to hydrothermal fluids and normally occur at high temperatures. The Mahallat hot springs are located in the north-eastern part of Mahallat city, in the highlands. These hot springs emerge through travertine and alluvial deposits. As noted, the area is extremely faulted, and the fractures enable an effective circulation of the water in the geothermal system. For this reason, the Mahallat hot spring waters are called faulted fountains. Water discharge from the fountains varies between 42 and 45 m^2/s. The negligible variance of water discharge, high temperature, and high partial pressure values of carbon dioxide represent deep hot springs in the Mahallat geothermal zone (Oskooi *et al*., 2016; Yazdi *et al*., 2016).

As illustrated in Fig. 3, a significant number of measuring stations in profile B are located on the Quaternary travertines and young terraces. On the contrary, the stations belonging to profile A are set on the Triassic dolomites, Pliocene conglomerates and sandstones, and Quaternary travertines. Many faults in the study area also facilitate the geothermal fluid transmission through the fractures of the limestone, dolomite, travertine, sandstone, and conglomerate formations. The Mahallat hot springs are situated at approximately 15 km from Mahallat city. Of note is the fact that the MT profile B has been designed on an almost steep slope topography, while profile A crosses a higher altitude with a gentle slope. The elevation gradients of profiles A and B range from 1,600 to 2,000 m and from 1,450 to 1,850 m, respectively.

3. Methodology

Inverse modelling of geophysical data means solving an optimisation problem to retrieve physical properties of subsurface structures. Generally, through the inversion process, an initial model is considered. The proper fitting between the observed and predicted data is determined

by numerical methods, and the model parameters are, accordingly, calculated with an appropriate error rate. In fact, adjustments applied to the forward modelling are controlled systematically to gain a proper misfit between the data and the observed model. A well-known solution for inverting MT data is the Tikhonov correction function (Tikhonov *et al*., 1977).

Rodi and Mackie solved the non-linear inverse problem for MT data by improving Newton's repetition algorithm and linear gradients. The following non-linear conjugate gradient (NLCG) algorithm was introduced to invert MT data (Rodi and Mackie, 2001). The mentioned approach leads to rapid inversion results obtained from the NLCG algorithm.

A general form of inverse problem can be considered as (Rodi and Mackie, 2001):

$$d = f(m) + e \tag{1}$$

where:

$$d = [d^1 d^2 \dots d^N]$$
$$m = [m^1 m^2 \dots m^M].$$

Correspondingly, *d* is the data vector, *N* is the number of data, *m* is the vector of unknown parameters, and *M* is the number of model parameters. In other words, for MT data, *M* is the number of resistivity blocks underneath the Earth's surface. The error vector is indicated with *e*, and the forward modelling function with *f*. The NLCG algorithm benefits from conjugate gradients to solve non-linear optimisation problems directly. The cost function used in the NLCG method is the Tikhonov function. Summarily, the NLCG utilises parametric series such as Eqs. 2, 3, and 4, respectively:

$$m = m_0 \tag{2}$$

$$m_{k+1} = m_l + \alpha_l p_l \quad k = 0, 1, 2, \dots \tag{3}$$

$$\Psi(m_l + \alpha_l p_l) = min\Psi(m_l + \alpha_l p_l) \tag{4}$$

where m_0 is the initial starting point of the algorithm or the initial model, which is generally considered as a homogeneous half space; *k* is the number of calculations; a_l is the step length; p_k is the line surfing, which is calculated through Eqs. 5 to 7:

$$\alpha_{l,k+1} = \alpha_{l,k} - \frac{g_{l,k}^T p_l}{p_l^T H_{l,k} p_l} \tag{5}$$

$$p_0 = -c_0 p_0 \tag{6}$$

$$p_l = c_l g_l + \beta_l p_{1-l} \quad l = 1, 2, \dots \tag{7}$$

In the above formulae, *c* and *g* are pre-conditions to increase the convergence rate and *g*

stands for the gradient operator. Through the Ribiere and Polak approach (Eq. 8), the conjugate gradient yields are determined (Smith and Booker, 1988):

$$\beta_l = \frac{g_l^T c_l (g_1 - g_{l-1})}{g_{l-1}^T c_{l-1} g_{l-1}}. \quad (8)$$

In order to minimise the cost function, determining parameter α is essential for the procedure, as well as for the gradient matrix calculation (Tikhonov *et al*., 1977).

Forasmuch as the relationship of the MT data and model parameters is non-linear, for minimising the function below, the utilisation of a proper iterative method would be a wise choice (Rodi and Mackie (2001):

$$\psi = [d - F(m)]^T V^{-1} [d - F(m)] + \tau m^T R^T R m. \quad (9)$$

To proceed with the minimisation process (Eq. 9), various modelling techniques can be employed, among which the NLCG algorithm. Therefore, Winglink software was used in this study to smooth the MT data and invert the data by means of the NLCG and sharp boundary techniques. Importantly, this software adopts the above mathematical techniques as built-in algorithms.

With lack of sharp gradients, the principle of smooth inverse modelling is based on the smooth variation of the resistivity values within the modelling space. Compared to geological features, this assumption may, occasionally, restrict the resolution of the inverse modelling process and provide unrealistic results. In order to avoid undesirable consequences, the sharp boundary inversion method, which utilises an initial 2D layered model with a homogeneous resistivity background and various thicknesses, can be adjusted to suit the specific case. The initial layering depths determine the layer boundaries within a set of nodes; the resistivity values for each layer are identified through the proper condition of the nodes. Therefore, node resistivity and depth are unknown parameters in the inversion process. By interpolating the estimated values between the nodes, the layer boundaries and resistivity values are found. Several studies dedicated to the use of sharp boundary inversion have been made (Smith *et al*., 1999; DeGroot-Heldin and Constable, 2004). In the sharp boundary method, worthy of note is that the number of unknown parameters (i.e. the depth and resistivity values of the nodes) is smaller than in the smooth inversion approach (Sarvandani *et al*., 2017). Contrary to the smooth inversion approach, the homogenous half-space initial model is not permitted in sharp boundary inversion procedures; thus, an initial layered model is utilised. Therefore, the use of this technique can be very useful in the characterisation of the shallower layered media, as well as in the correct applicability in sharpening the subsurface edges and contrasts. When reviewing background geological information and multiple geophysical aspects, sharp boundary models can introduce higher subjectivity levels to the modelling process, through the use of pre-defined medium by the interpreter.

Basically, arbitrary and complicated 2D models can be defined by determining the resistivity of various geological units and their boundary positions at some point along their lengths. In the sharp boundary method, the layered models can have variable lateral thicknesses, so that the layer border can be determined by n_n nodes and their interpolations. Therefore, for a model with n_b interference, a long vector, known as $n_b \times n_n$, is composed with the model parameters (m) (Smith *et al*., 1999). While layer resistivity is unknown, $n_b + 1$ (where n is the number of

unknown layers added to one homogeneous half-space medium) values of ρ_j can be attached to vector m. Since the layers can have lateral variable resistivity values, the resistivity of each layer is determined at n_n and interpolation is conducted laterally; subsequently, other parameters are added to model m (Eq. 9):

$$\left[z_{11}, \dots, z_{1n_n}, \dots, z_{n_b n_n}, log(\sigma_{11}), \dots, log(\sigma_{1n_n}), \dots, log(\sigma_{n_b n_n})\right]^T \tag{10}$$

where z_{ij} is the depth of the j-th node at the i-th interface, T is the transpose vector, and ρ_{ij} is the resistivity of the i-th layer at the j-th point.

As the parameterisation of the model is completed, the inversion would be fulfilled by minimising a cost function. As discussed, for the layered models containing various thicknesses and resistivity values, the border of each layer is defined as $z_{i(x)}$, a continuous function of the horizontal points. The function below (Eq. 11) must be minimised:

$$\int \left[\frac{d}{dx} z_1(x)\right]^2 dx + \cdots + \int \left[\frac{d}{dx} z_{n_b}(x)\right]^2 dx + \beta \lceil r \rceil^2. \tag{11}$$

For determined models with limited parameters, the differentiation and integrals can be estimated by means of the finite difference approach or other additional methods. To define roughness matrix R_m, Eq. 12 is expressed as:

$$\begin{bmatrix} \frac{-1}{\Delta x_{11}} & \frac{-1}{\Delta x_{11}} & 0 & \dots & 0 \\ 0 & \frac{-1}{\Delta x_{12}} & \frac{1}{\Delta x_{12}} & \dots & 0 \\ 0 & \dots & 0 & \dots & 0 \\ 0 & \dots & \dots & \dots & \frac{1}{\Delta x_{n_b n_n - 1}} \end{bmatrix}. \tag{12}$$

Weighting of the rows in the roughness matrix is conducted through the use of the distance inverse, as given by the relation $\Delta x_{ij}^{-½}$, leading to weighting the squared components of matrix R_m by relating length intervals Δx_{ij}, so that the term $|R_m|^2 = m^t R^t R_m$ estimates the sum of the integrals in Eq. 11. In the sharp boundary inversion approach, in order to weight the differentiation estimation, the matrix given below is utilised so that $w_i \equiv w_{i1} = w_{i2} = \dots = w_{in_n - 1}$:

$$R_b = \begin{bmatrix} -w_{11} & w_{11} & 0 & \dots & 0 \\ 0 & -w_{12} & w_{12} & \dots & 0 \\ 0 & \dots & 0 & \dots & 0 \\ 0 & \dots & \dots & \dots & w_{n_b n_n - 1} \end{bmatrix}. \tag{13}$$

The model roughness matrix, including the $n_b \times n_n$ columns and $n_b \times (n_n - 1)$ rows, is defined, so that:

$$R = \begin{bmatrix} R_b & 0 \\ 0 & R_c \end{bmatrix} \tag{14}$$

where R_c with a different weighting set (w_i', i = 1, ..., n_b) can also be transformed to the style of R_b (Eq. 13).

To vary the layer conductivity model laterally, while minimising (Smith *et al.*, 1999):

$$|Rm|^2 + \beta|r|^2. \tag{15}$$

The relative intensities of weights w_i and w_i' are used to form R_b and R_c. Considering the non-linear model parameters in MT data, the iterative method would be a good choice to minimise Eq. 15. The apparent resistivity and phase will be calculated for n_s measuring sites and n_f frequencies, as elements of n_d extended data vector $d^{(obs)}$, and the response of a model m as d.

Linearising around m_i achieves:

$$d - d_i = F_i.(m - m_i), \tag{16}$$

where second-order terms in ($m - m_i$) have been ignored. Measured data residuals (r), as well as accounting for model response d as vector, would read:

$$r \equiv d^{(obs)} - d \tag{17}$$

which is the remaining measured data according to model response d as a vector. Utilising Eq. 16 (linearisation) provides:

$$r = d' - F_i m_i, \tag{18}$$

So that

$$d' \equiv d^{(obs)} + F_i m_i - d_i, \tag{19}$$

on the i-th iteration. In Eq. 15, the above equation is used for r as a function of parameter m. The minimum of Eq. 15 would be a stationary point respecting δm, thus:

$$r + \delta r = d' + F_i \cdot (m + \delta m). \tag{20}$$

It is worth noting that the δm coefficient must be eliminated (Smith *et al.*, 1999). So,

$$(\beta F_i^t f_i + R^t R)m = \beta F_i^t d'. \tag{21}$$

This would be the $n_p \times n_p$ expression for n_p model parameters. This equation can be employed to call a new model parameter m for every iteration. The sharp technique iteratively approaches the minimum of Eq. 14, starting at a certain m_i model, by calculating partial derivative matrix F_i numerically at m_i, and solving Eq. 21 for an estimated new model, $m_{i+1} = m$. Eq. 21 is entrenched

in linearisation (Eq. 16), which considers that the changing in the model ($\hat{m}_{i+1}$ - m_i) is small enough to ignore second-order terms in ($\hat{m}_{i+1}$ - m_i). An iteration is considered successful if, in calculating response d_{i+1} of model m_{i+1}, the objective Eq. 15 decreases for the current β value, i.e. if (Smith *et al*., 1999):

$$|Rm_{i+1}|^2 + \beta|r_{i+1}|^2 \leq |Rm_i|^2 + \beta|r_i|^2. \quad (22)$$

As the model where the partial derivatives are evaluated (i.e. m_i) may still not be at the minimum of Eq. 15 for any amount of β, adjusting β and recalculating m_{i+1} does not ensure that ($\hat{m}_{i+1}$ - m_i) can be small enough for Eq. 22 to be valid for $m_{i+1} = \hat{m}_{i+1}$. Taking a partial step in the desired orientation, allowing:

$$m_{i+1} = m_i + \alpha \cdot [\hat{m}_{i+1} - m_i] \quad (23)$$

with $0 < \alpha \leq 1$, a small enough α value can be chosen so that Eq. 22 can be valid for m_{i+1}, assuming that Eq. 21 is non-singular.

Smith and Booker (1988) provide a simple criterion for choosing between decreasing α and decreasing β to reduce the step size. In their expression, the squared misfit can be written as a function of trade-off parameter β with the form of:

$$|\hat{r}_{i+1}(\beta)| = \sum_{k=1}^{n_d} \left(\frac{\gamma_k}{1+\beta\lambda_k}\right)^2 \quad (24)$$

where $\lambda_k \geq 0$ and γ_k are known, for estimated model $\hat{m}_{i+1}(\beta)$ considered as a function of β, with regards to linearisation similar to Eq. 16 (Smith, 1999).

4. Results

4.1. Synthetic model simulation

In order to correctly investigate and compare the different inverse modelling techniques, and also study the resolution of the smooth and sharp boundary models, a synthetic scenario was initialised, while the MT forward model responses [Transverse Electric (TE) and Transverse Magnetic (TM) resistivity and phases] were calculated through the finite element approach. To consider ambient noise, 5% Gaussian noise was added (DeGroot-Hedlin and Constable, 2004). The Lagrange coefficient (τ), the weight coefficient controlling the horizontal and vertical roughness (α and β) of the model parameters, and the minimum dimension of the blocks in the ratio of horizontal and vertical directions (H/V) were obtained using the L-Curve diagram. It is worth noting that a 1% error floor for resistivity and phase data was considered for the synthetic model presented.

This synthetic model was adopted to apply the sharp boundary settings to the predefined layered model in order to investigate its applicability and precision in comparison to the smooth inversion scheme. The regularised smooth inversion of MT data has been applied to the initial half-space model with a 100 Ωm resistivity. The designed synthetic model belongs to a solid

conductive layer (10 Ωm) bounded by two layers. The resistivity of the surface layer is 1,000 Ωm, and a 100 Ωm resistivity is also considered for the other layers. Figs. 5 and 6 depict the MT response sections, illustrating the outcomes of the sharp boundary approach.

A smooth inversion model, with an initial 100 Ωm homogeneous half-space, has been constructed. The results of the numerical analysis provide the optimised values for τ, α, β, and H/V, which are 10, 0.5, 0.5, and 500/500, respectively (Fig. 4).

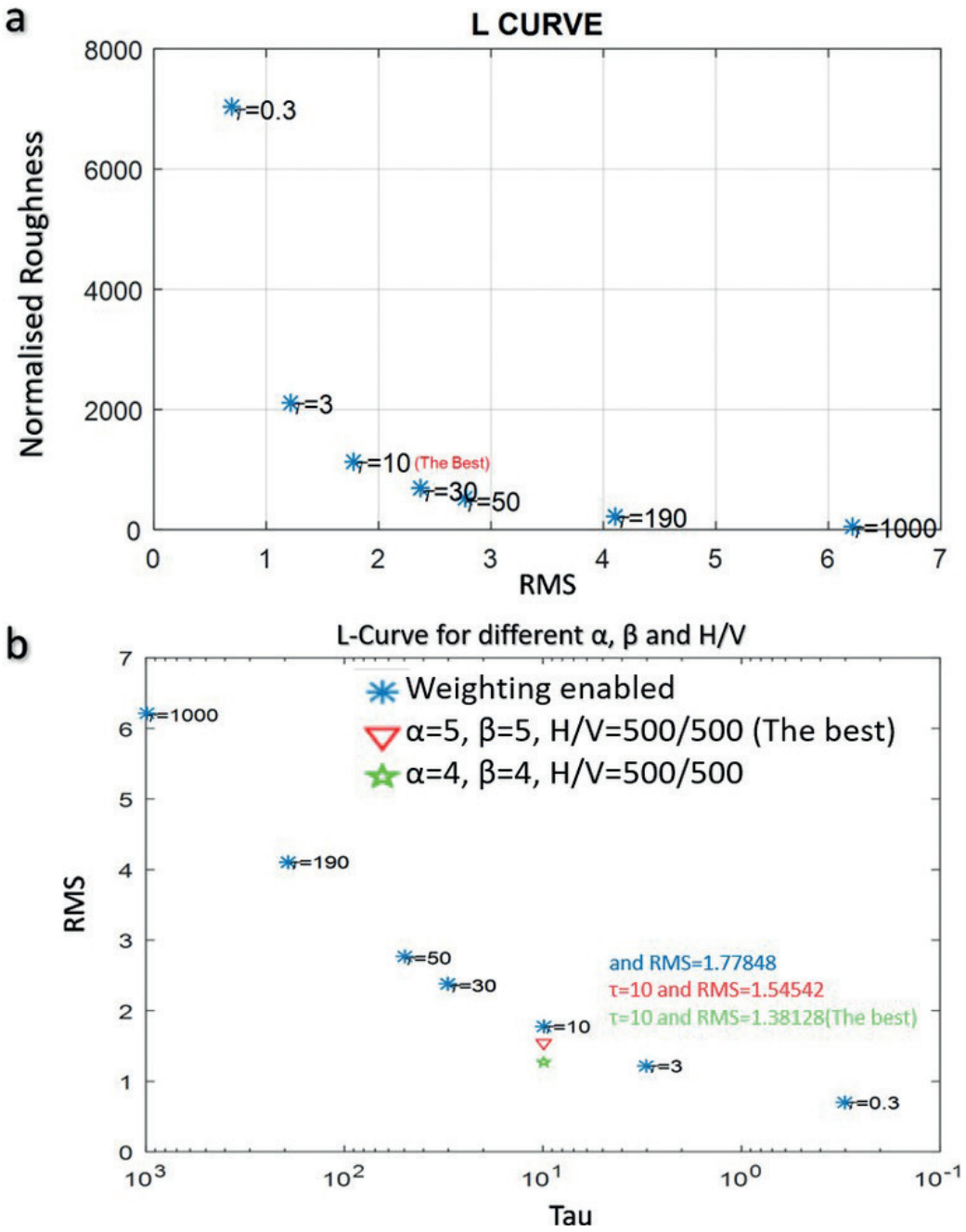

Fig. 4 - L-Curve diagram of the synthetic model.

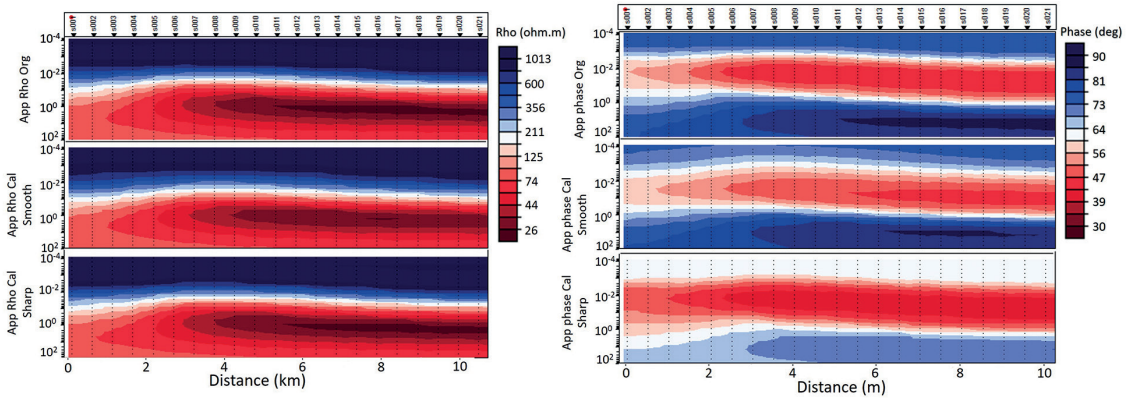

Fig. 5 - TE mode data along the synthetic model including observed and calculated sections. A bimodal data inversion was executed (TE+TM).

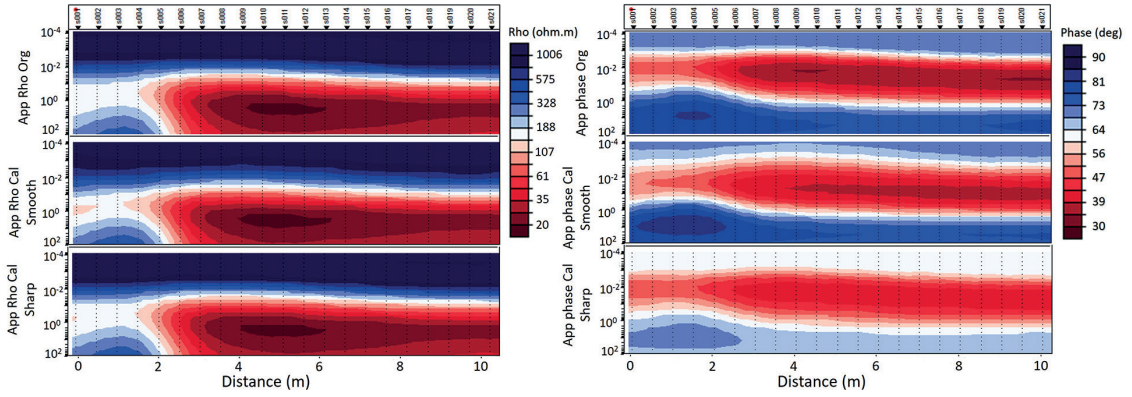

Fig. 6 - TM mode data along the synthetic model including observed and calculated sections. A bimodal data inversion was executed (TE+TM).

In order to assess the precision of the smooth and sharp boundary inversion schemes, pseudo-sections of apparent resistivity and phase, both for observed and calculated data, are depicted in Figs. 5 and 6. The pseudo-sections (TE and TM modes) in these figures reveal acceptable results from the inverse modelling process, both in terms of observed and predicted data.

As illustrated in Fig. 7a, a three-layered synthetic model with a notable resistivity gradient is simulated. This scenario presents the superiority of sharp boundary inversion over smooth inversion. Although the RMS factor for smooth inversion (Fig. 7b) is 1.38, a reasonably acceptable value, the smooth model does not show realistic accommodation with the geoelectrical features initially considered. Clearly, the bottom and top of the conductive layer, as well as the non-realistic resistive structure in a depth of 2 to 4 km, is not precisely recovered. Under the mentioned circumstances, sharp boundary inversion can be the preferred method to achieve more accurate inverted models. It is worth noting that the 1D or 2D inversion results, initial geological data, and other geophysical methods can be utilised to adjust the sharp boundary inversion procedure. If geological information, results from previous studies or other geophysical models (such as smooth inversion sections) are available, the interpreter can introduce realistic constraints in the inversion algorithm. This serves to limit the non-uniqueness of the model, enhancing the

incorporation of existing knowledge and improving the reliability of the inversion results. All these provide important preliminary information about the geometry of the sought target.

In the following, the inversion technique is applied to a three-layered model with features as given in Table 1. The position of the nodes and the resistivity of each layer are shown in Fig. 7c. The final result of the sharp boundary inversion is, also, depicted in Fig. 7d. Although the left side of the sharply inverted model is not intercepted in the proper location, the result indicates that the resistivity values, the layer borders, and the dip of the layer bottom and top have been ideally recovered. Conversely, the spurious structures are not generated in the models. As can be observed, in the synthetic simulation illustrated, the smooth inversion result (Fig. 7b) produces undesirable artefacts above the conductive layer, along with a deep conductive artefact below it. It can be stated that the regularised smooth inversion result has not been able to properly recover the interface boundaries between the high conductive zone and the above resistive layer.

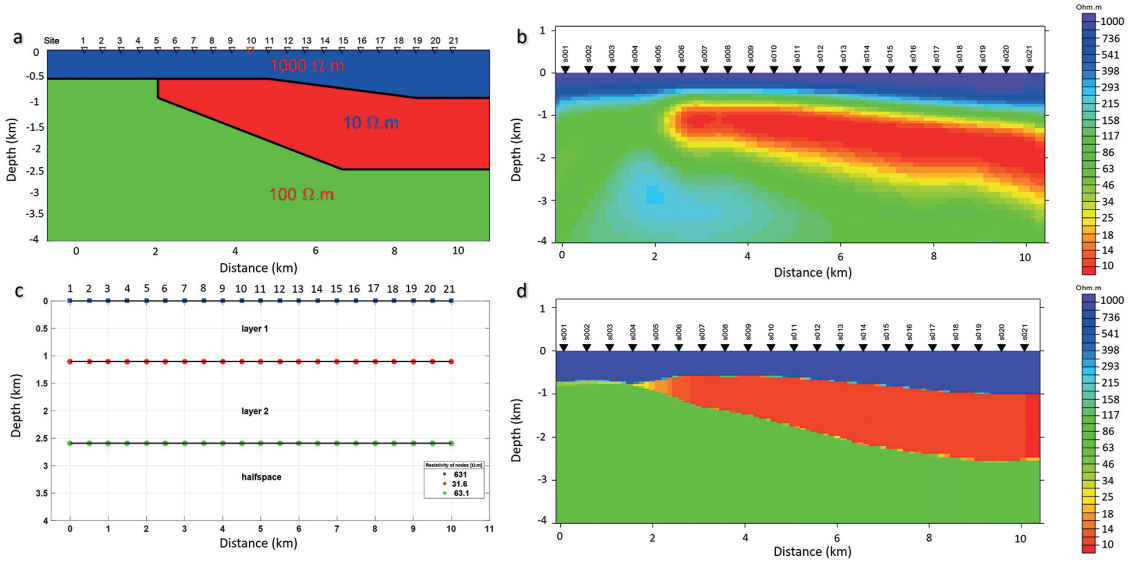

Fig. 7 - A synthetic model simulation through electrical resistivity property: a) synthetic model, b) smooth inversion model, c) electrical resistivity layering definition for executing sharp boundary inversion, and d) sharp boundary inversion model.

4.2. MT survey

As indicated in Fig. 3, the MT survey on the Mahallat geothermal field was conducted on two almost perpendicular profiles of A and B, with 12 and 17 stations respectively, in July 2011. Overall, 29 MT measurement stations were established through frequency ranges from 0.008 to 8,000 Hz. A 500-metre spacing between adjacent sites is considered to maintain the survey data resolution.

4.2.1. MT data analysis

Prior to feeding MT data into the inversion algorithm, a series of procedures aimed at preparing the data in a format suitable for the algorithm execution must be performed. These procedures

Table 1 - Assumed parameters for synthetic data inversion.

Smooth Inversion	Model	Tau	α	β	H/V	RMS	Iteration	Error Floor (%)			
								TM		TE	
								Rho	Phase	Rho	Phase
	Synthetic model simulation	10	0.5	0.5	500/500	1.38	100	20	7	20	7
Sharp boundary Inversion	Model	Tau for resistivity	Tau for interface	Damping factor	RMS						
	Synthetic model simulation	30000	35000	0.3	1.47						

are carried out to enhance performance and ensure a proper evaluation of the results. In order to conduct a qualitative study on MT data, determination of the geoelectrical strike is an extremely important part of inverse modelling. For this reason, pseudo-sections of skew angles and phase tensor ellipsoids are represented in Fig. 8. Generally, negligible skew angles can be considered as a representation of a 2D structure. Consequently, in the pseudo-section of profile A, the 3D structure distortion effects, within shallow depths, can be perceived. In contrast, as the depth is increased (for periods longer than 0.01 s), 2D structures appear, and the smaller skew values confirm this. In profile B, the 3D distortion effects are more marked; however, the 2D structures are quite dominant in the related pseudo-sections.

Fig. 9 shows the Niblett-Bostick penetration depth for stations within profiles A and B, by indicating the penetrating depth variation in different periods (Niblett and Sayn-Wittgenstein, 1960; Bostick, 1977). The left and right columns, corresponding to each station, show the TE- and TM-mode data, respectively. As clearly shown, by increasing the periods, signal penetrations are expanded. The analysis of the penetration depth sections for both profiles reveals that MT data offer reliable information about subsurface structures to a depth of at least 10 km. The considerable differentiation between penetration depth values in the TE and TM modes explains the structures with various resistivity values underneath the stations.

According to the Swift skew, Bahr, and phase tensor results, as well as the phase tensor ellipsoid results, distortion effects due to the surface 3D conductive layers can be observed in periods longer than 1 s and shorter than 0.01 s. Considering the data analysis results, along with the results of previous studies in the area, a general 2D geoelectrical structure, which was proposed by Oskooi *et al*. (2014), could be appropriately approved (Fig. 10).

Fig. 10 depicts an illustration of the phase tensor of profiles A and B. The colours of the ellipsoids represent the skew angle (β) and facilitate the interpretation of the phase tensors and underground dimensionality of the Mahallat zone. Briefly, if the absolute values of skew angles range within 0 to 5, statistically, a 2D strike can be considered for the subsurface structures. As can be observed, for profile A, the stretched ellipsoids signify the 2D within major sectors of the section. Notably, the minor values of the skew angle, corresponding to the 2D structures, confirm the 2D interpretation. In Fig. 10b, as previously discussed, the 3D structures have partly influenced

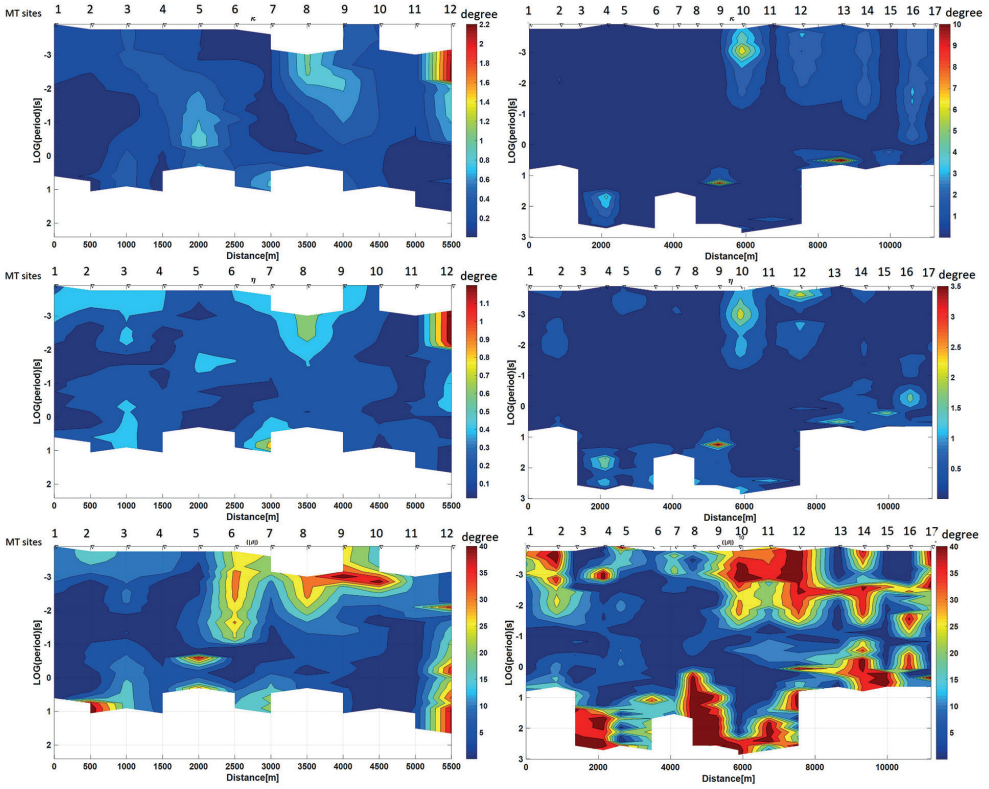

Fig. 8 - Skew plots along profile A (first column) and profile B (second column), where the first row, second row, and third row are plotted, respectively.

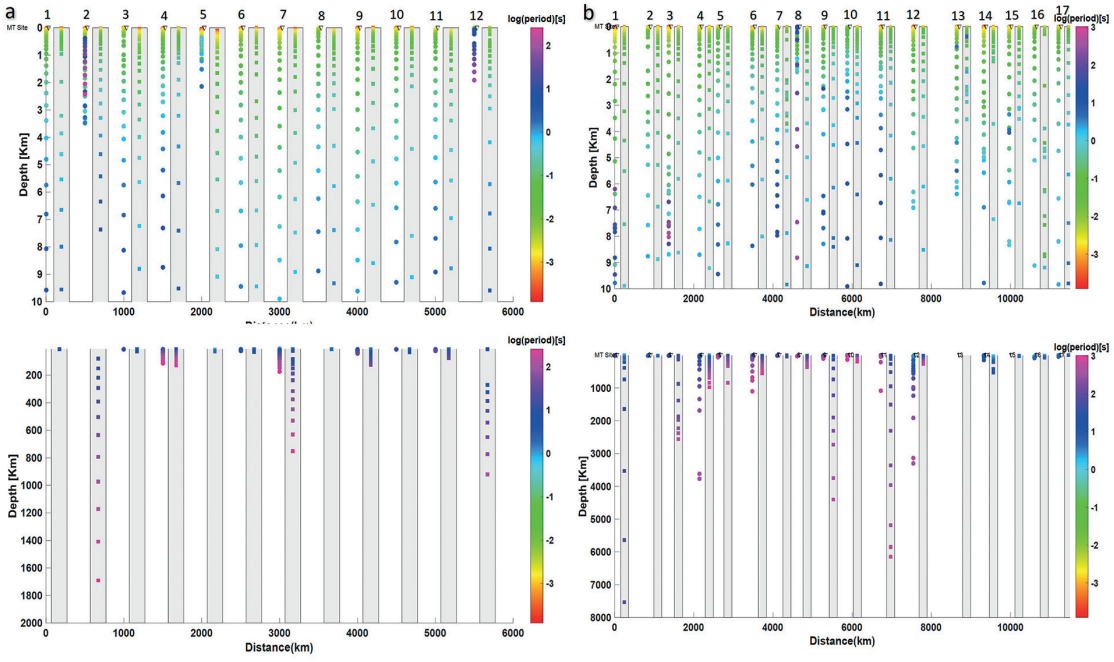

Fig. 9 - The Niblett-Bostick penetration depth for each station within profile A (a) and B (b).

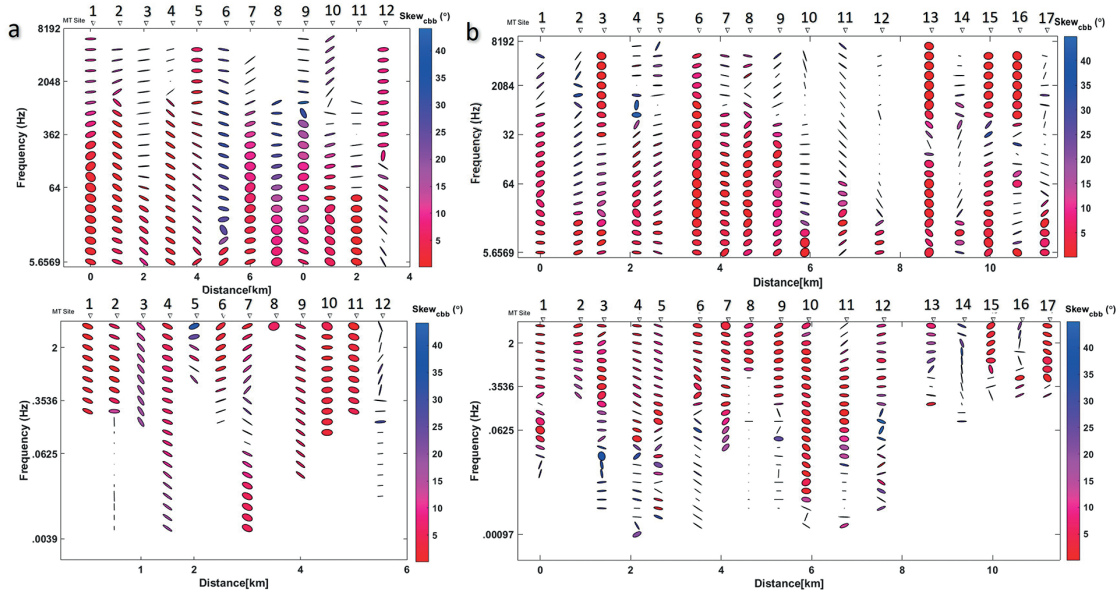

Fig. 10 - Phase tensor plots along profiles A (a) and B (b).

the data, which is obvious at some of the ellipsoids. Nonetheless, a significant number of normal ellipsoids, indicating the 2D behaviour of the data at the majority of sites and periods, can be seen in the sections. Thus, even though the 3D distortion effects are evident, overall stretched ellipsoids represent the general 2D structures within subsurface layers (Caldwell, 2004).

Fig. 11 indicates the rose diagrams, which are calculated by the swift and phase tensor methods for both profiles (Vezoff, 1972; Caldwell, 2004). Due to the existence of 90° ambiguity in the MT process, in addition to the calculated strike of the area, perpendicular strikes are also

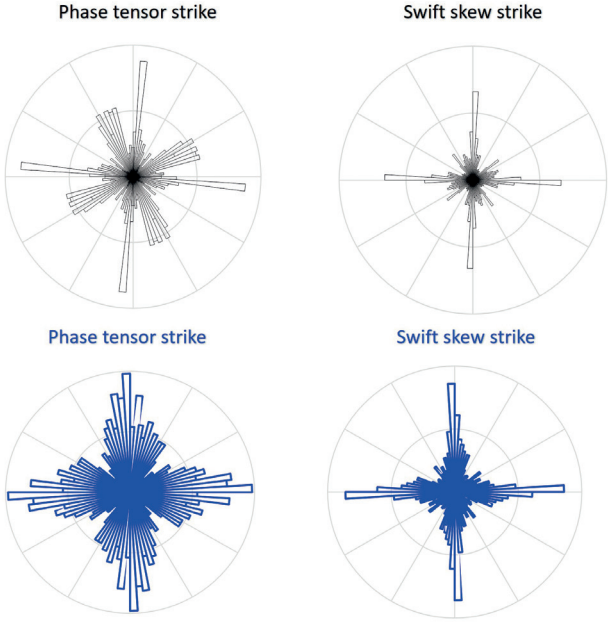

Fig. 11 - Rose diagram plots delineating geoelectrical strike directions along profile A (first row) and profile B (second row).

exhibited. Ultimately, an orthogonal geoelectrical strike orientation, with almost zero degrees of deviation, is determined for the general strike of the study area, also confirming the results of previous studies. As stated, the estimated strike holds a 90° ambiguity. Despite the presence of relatively high scattering, the type of distribution of the directional values makes it possible to select a dominant direction. Calculating the directional mean of the resulting values and, also, considering the geological information, such as the N-S trend of the Mahallat active fault in the region (along with a review of the previous studies in the region), can contribute to selecting the final direction of a unique geoelectrical strike within the study area for the purpose of performing a 2D inversion (Hosseini *et al*., 2021). Noteworthy are the distortion effects of the data that are obviated by 2D Groom-Bailey tensor decomposition. The twist and shear histograms indicate high distortion effects (Fig. 12).

4.2.2. MT data inversion

Following the dimensionality analyses, geoelectrical strike determination, outlier data correction (through D+ criterion adjustment), and 2D inverse modelling (within the regularised

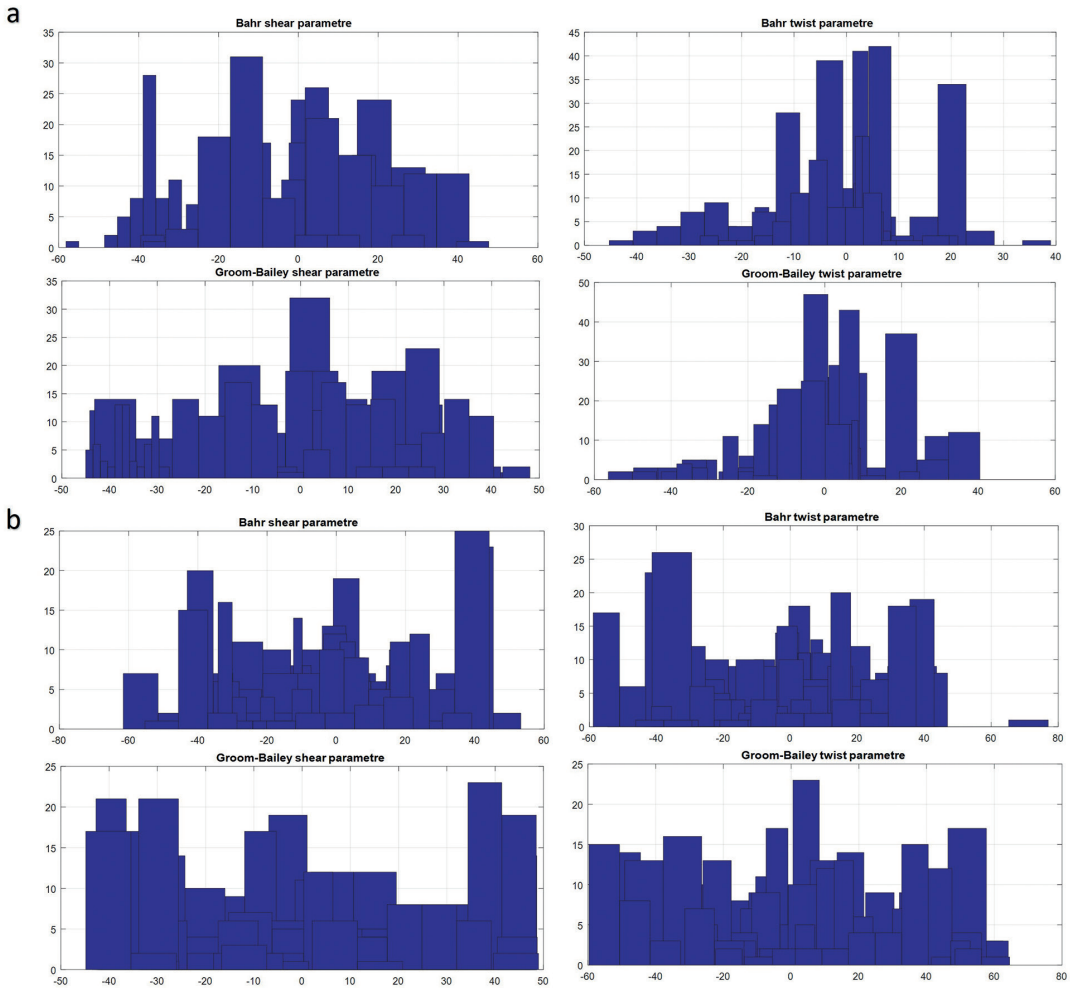

Fig. 12 - The distortion parameters correspond to profile A (a) and profile B (b).

smooth and sharp boundary approaches) have been conducted. In this regard, the Lagrange coefficient (τ), weighted coefficient (α, β), and block minimum dimensions (H/V) are calculated through L-Curve diagrams.

Prior to illustrating the 2D inverted models for each profile, the resistivity pseudo-sections of the profiles are presented. As clearly shown, the pseudo-sections are related to both the TE and TM modes. Figs. 13 and 14 represent the pseudo-sections of profile A for the TE and TM modes, respectively. The figures correspond to the smooth inversion observed and predicted data along with the predicted sections of smooth and sharp boundary inversions. In addition, Figs. 15 and 16 represent the pseudo-sections of profile B for the TE and TM modes accompanied by the smooth inversion observed and predicted data, and sharp boundary predicted data. Based on the results, it can be asserted that the 2D inverse modelling scheme, for each profile, yields reasonable fits to the data. The corresponding RMS inversion values serve as a precision measure of the inversion results.

A smooth inversion of profile A, with an initial homogeneous half-space of 100 Ωm, Lagrange coefficient of three (τ = 3), α and β equal to 0.5 and 0.7, and H/V ratio of 300/300, has been conducted (Fig. 17). Along profile A, a conductive zone underneath stations nos. 1 to 4 could be

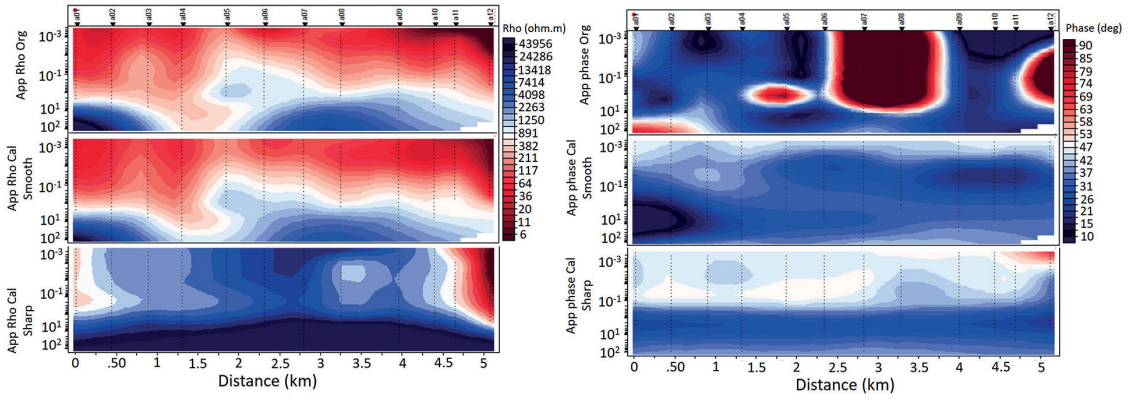

Fig. 13 - TE mode from MT data along profile A over the Mahallat geothermal reservoir including observed and calculated sections. A bimodal data inversion was executed (TE+TM).

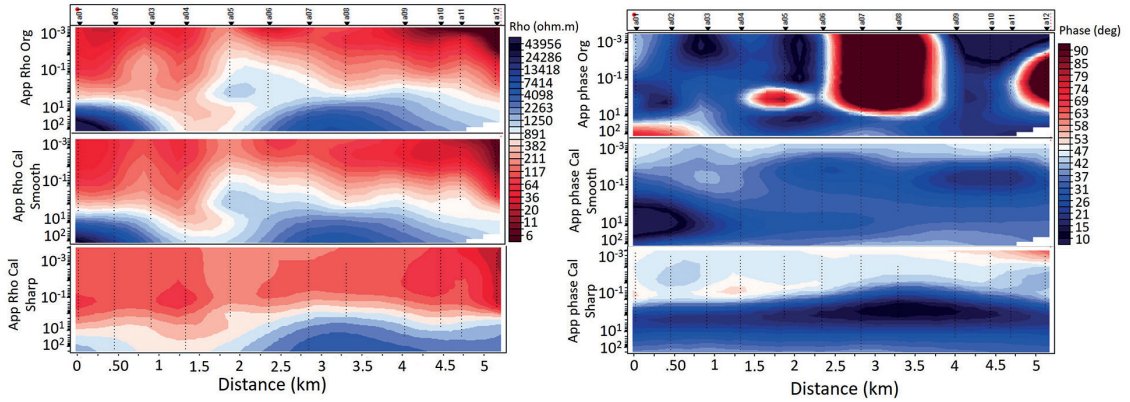

Fig. 14 - TM mode from MT data along profile A over the Mahallat geothermal reservoir including observed and calculated sections. A bimodal data inversion was executed (TE+TM).

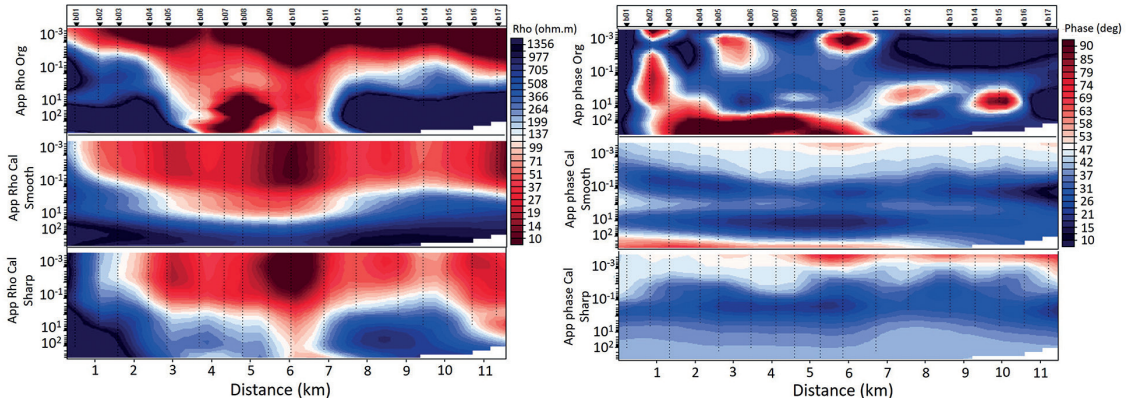

Fig. 15 - TE mode from MT data along profile B over the Mahallat geothermal reservoir including observed and calculated sections. A bimodal data inversion was executed (TE+TM).

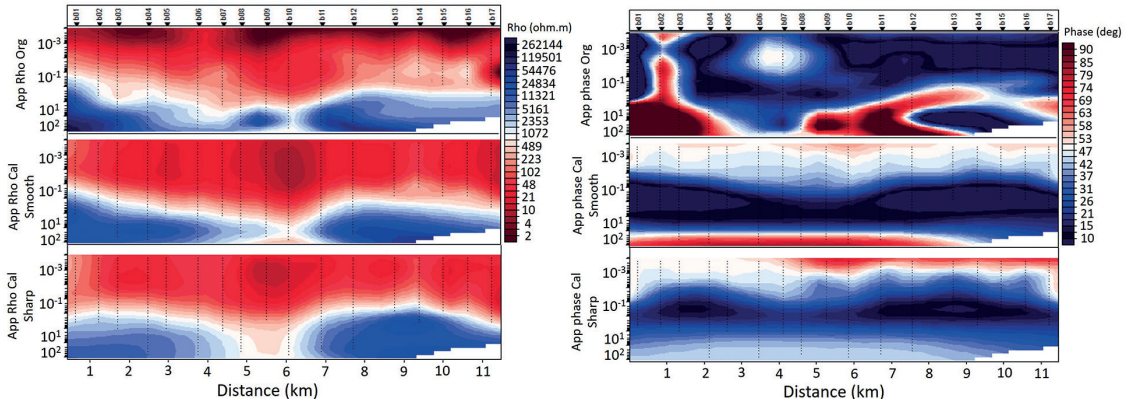

Fig. 16 - TM mode from MT data along profile B over the Mahallat geothermal reservoir including observed and calculated sections. A bimodal data inversion was executed (TE+TM).

observed (25 to 90 Ωm resistivity). This high-temperature conductive zone is located between two resistive zones (with more than 230 Ωm resistivity) corresponding to the intrusive volcanic bodies. Additionally, beneath the mentioned stations and stations nos. 10, 11, and 12, a conductive layer could also be resolved at a depth from 1,400 to 1,800 m, interpretable as the conductive cap. Below the resistive zone, there is a relatively more resistive area (30 to 300 Ωm) related to the geothermal reservoir.

A smooth inversion of profile B, within an initial homogeneous half-space of 100 Ωm, has also been conducted. It took into consideration the following adjustment parameters: Lagrange coefficient of 4 (τ = 4), α = 0.5, β = 0.1, and H/V = 200/200. As can be inferred from the sections, in profile B, the conductive cap is detected under stations nos. 4 to 11 in depths from 1,500 to 1,800 m a.s.l., with 10 to 35 Ωm resistivity. Furthermore, underneath stations nos. 6 to 11, there is an obvious conductive zone (5 to 10 Ωm), among the resistive sectors, which belongs to the thermal source of the geothermal system. In addition, under the conductive cap and on the sides of the heat source, a relatively resistive zone (30 to 300 Ωm), can be attributed to the probable hydrothermal fluid reservoir.

Combining the results from Fig. 18 with the geological information and findings from

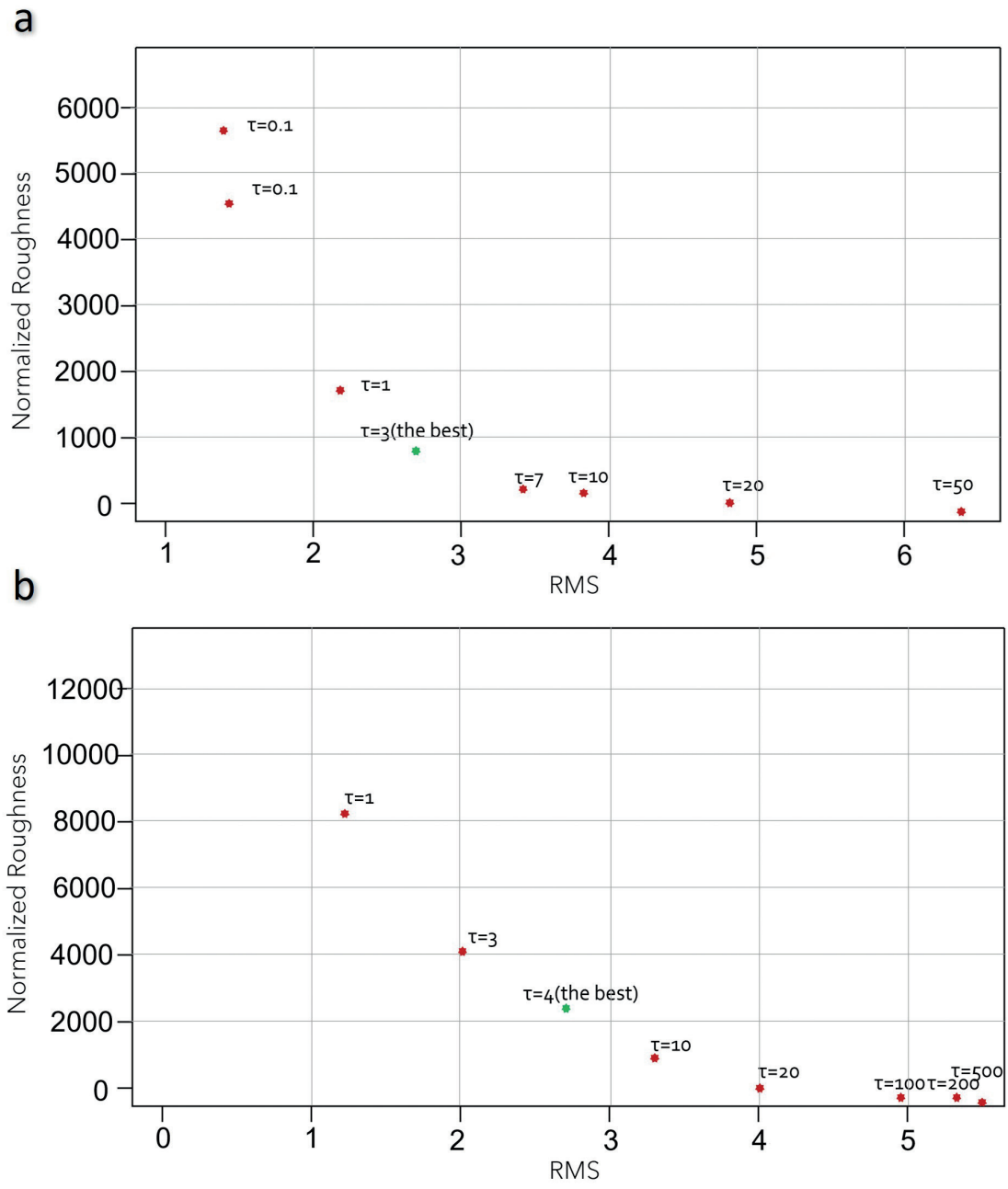

Fig. 17 - L-Curve diagram for profile A (a), and profile B (b).

previous studies, the smooth inverse models can be interpreted. This interpretation enables the positioning of the fault location over the structures, while focusing on the resistivity changes and/or discontinuities. A conductive zone is resolved beneath stations nos. 3 to 6 along profile A, which is also detected at stations nos. 7 and 8 along profile B. Several faults force the hot water to rise to the surface at some locations. According to the hot springs around stations A02, A03, A06, A07, A08, B02, B03, and B04, this extrusion can be attributed to the mentioned faults and fractures, which are also determined by the inversion results.

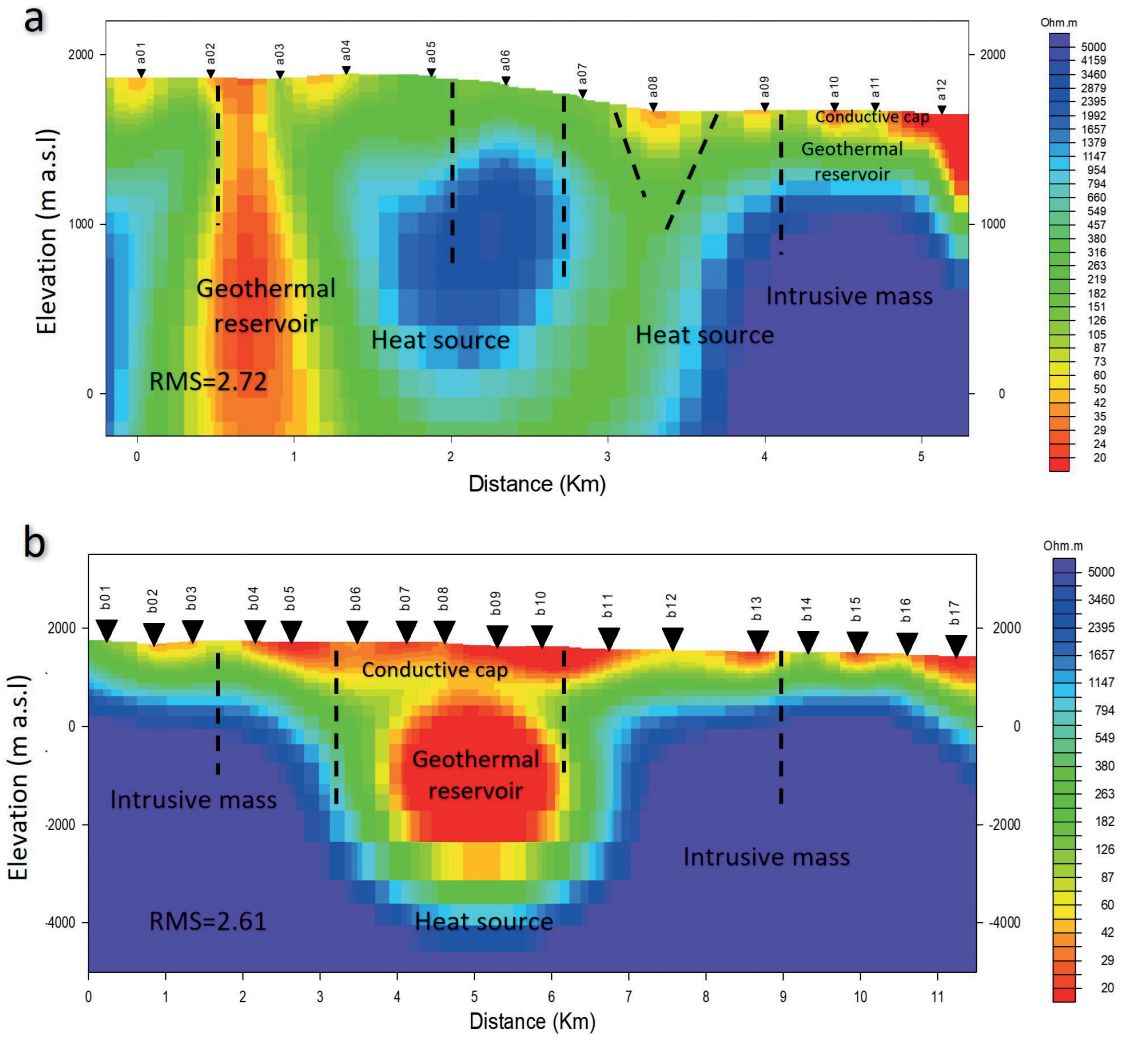

Fig. 18 - 2D smooth inversion results along with determination of the geothermal system components profile A (a), and profile B (b).

Generally, it can be concluded that the conductive surface layers are related to shallow sediments, young alluvium, and Quaternary travertines. The resistive layer under the surface, consisting of tuff and basalt, can be interpreted as the cap rock. Due to the presence of water and hot springs around the profiles, the geothermal reservoir shows a high conductivity response. Geologically, it is formed of Miocene limestone, as indicated by the geological sections and previous research of the area. The effective incorporation of as much geological information as possible into the geophysical inversion can lead to greater modelling accuracy, which will significantly increase algorithm performance.

Fig. 19 indicates the node locations for the sharp boundary inversion and the geological formation layering, with nodes positioned beneath the monitoring stations. By acquiring sharp boundary inversion techniques (Fig. 20), the results showcase the geothermal reservoir identified through smooth inversion, along with the prediction of the basement rock depth. This prediction aligns well with previous research. The smooth inversion has specified the basement rock depth

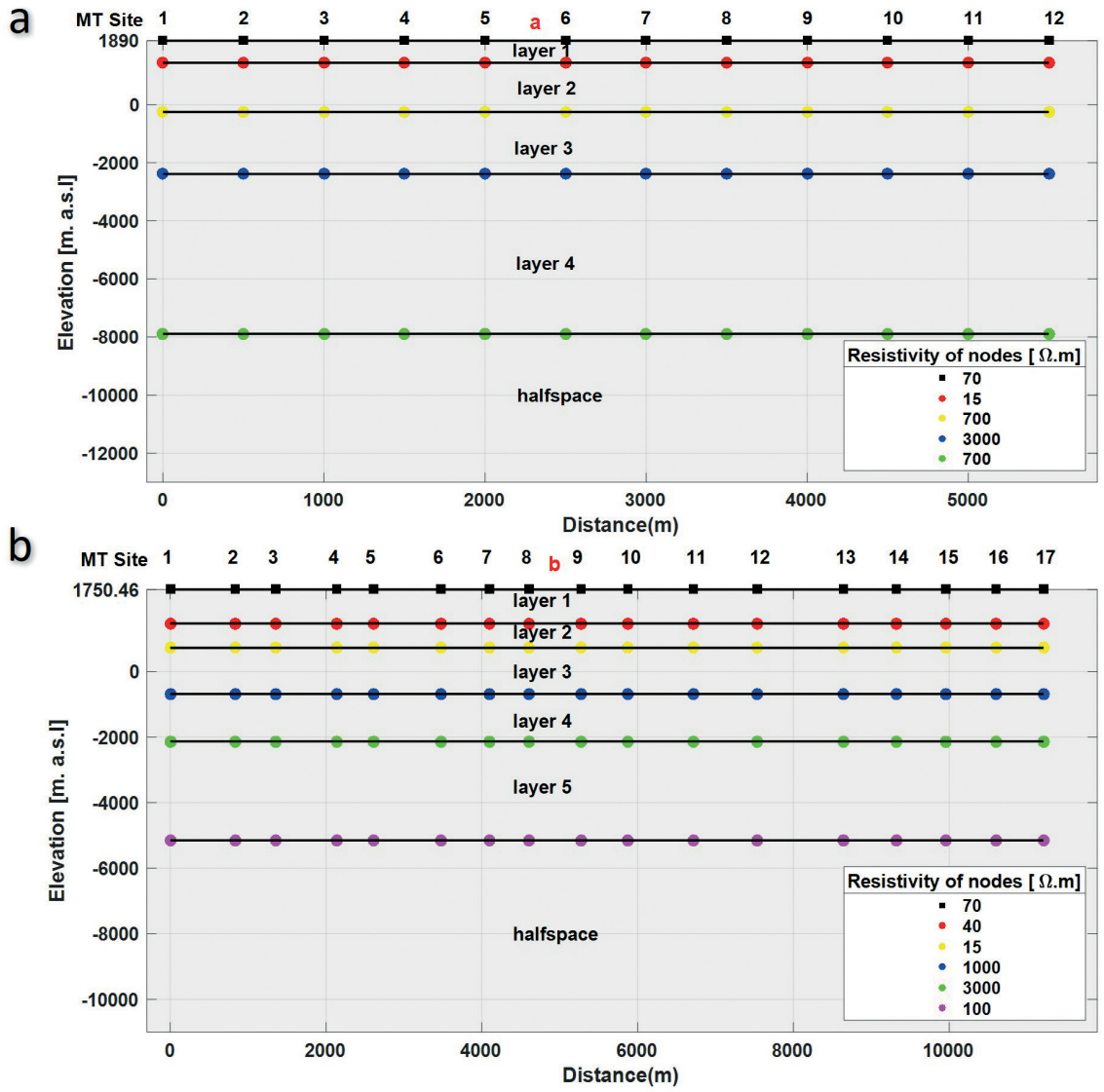

Fig. 19 - Electrical resistivity layering definition along profile A (a) and profile B (b) for executing sharp boundary inversion.

at approximately -4,000 m, while the sharp boundary inversions place it at -2,000 m, which is consistent with the geological section. Furthermore, the sharp boundary inversion results for profile A prove a conductive zone under stations nos. 10 to 12, which is expanded to -250 m according to the geological section. However, smooth inversion places this zone at greater depths, potentially deviating from the true geological structure. Additionally, a conductive thermal source is identified in the smooth inversion of profile A.

Table 2 represents the values of the required inversion parameters for profiles A and B in the cases of smooth and sharp boundary inversion methods.

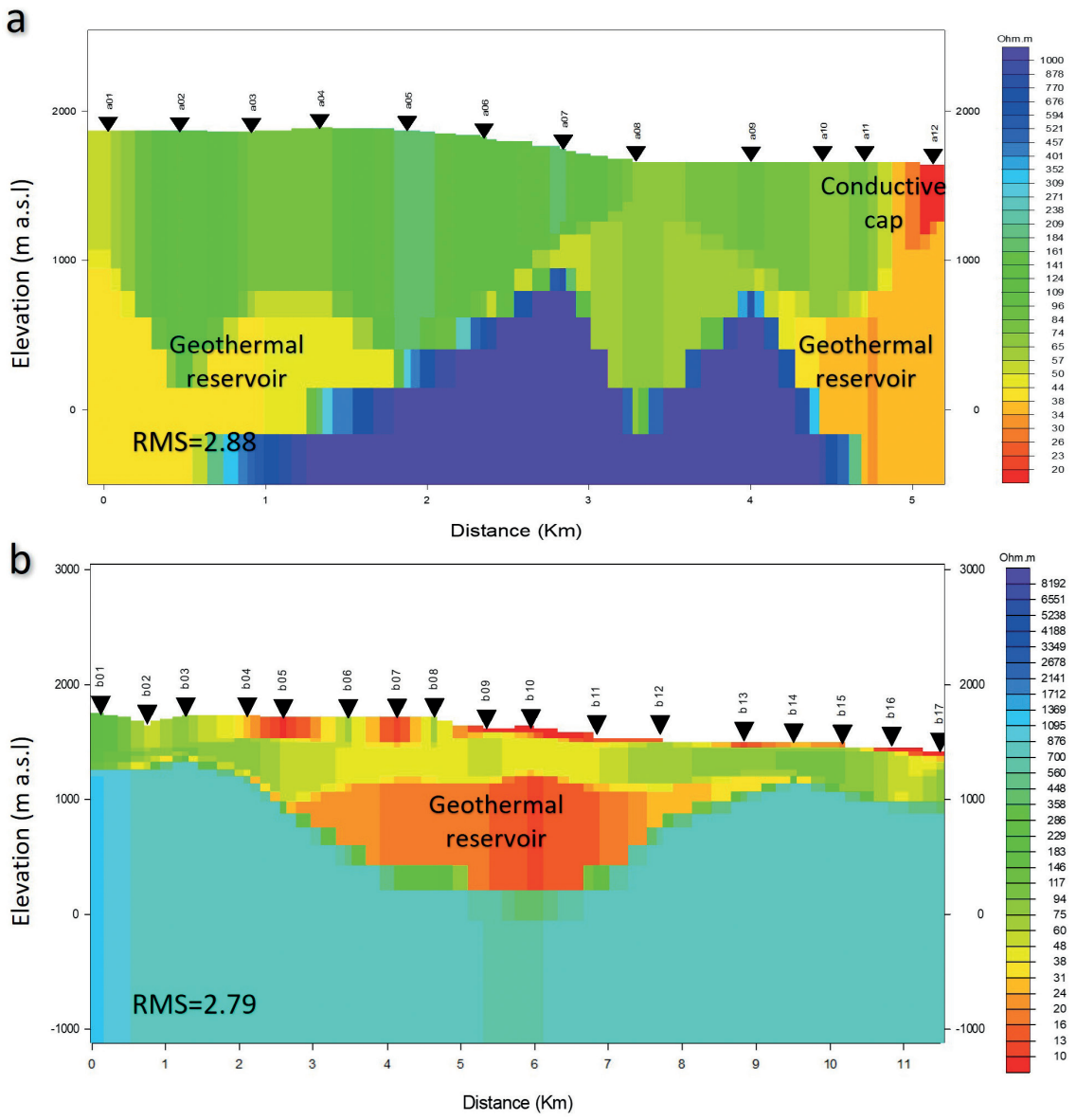

Fig. 20 - 2D sharp boundary inverted models along profile A (a), and profile B (b).

5. Discussion

As previously discussed, the main target, after inverse modelling, is to produce conceptual models on subsurface structures (Fig. 21). Accordingly, by following multi-method inverse modelling, based on the physical features and geological information, plausible geological models are provided. These models portray the subsurface structures of the study area and are fairly well synchronised with the geothermal attributes. The application of the multi-method inversion enables to specify the geothermal structures more accurately and update the geological sections in the Mahallat geothermal region. Initially, the authors undertook a smooth inversion procedure constrained by initial model resistivities and a designed mesh that

Table 2 - Assumed parameters for real data inversion.

Smooth Inversion	Profile	τ	α	β	H/V	RMS	Iteration	Error Floor (%)			
								TM		TE	
								Rho	Phase	Rho	Phase
	a	3	0.5	0.7	300/300	2.72	120	20	5	20	5
	b	4	0.5	0.1	200/200	2.61	100	20	5	20	5

Sharp boundary Inversion	Profile	Tau for resistivity	Tau for interface	Damping factor	RMS
	a	1	1	0.3	2.88
	b	1	1	0.3	2.79

considered geological information and findings from previous studies in the area (Oskooi *et al*., 2014, 2016; Hosseini *et al*., 2021). This involved the use of a finer mesh in prominent zones and a slightly sparser mesh in less prominent zones. Furthermore, the smooth inversions were iterated to generate an L-Curve diagram, to help identify the optimal point for the trade-off (τ) value between model roughness and RMS. Subsequently, the inversion parameters were determined through a trial-and-error process to minimise the RMS factor. Next, by relying on the results from smooth inversion, a plan for sharp boundary inversion was devised and the electrical node layers were identified. To achieve this, the initial geological information and insights from previous studies for the author's sharp boundary inversion problem were elaborated. Collectively, these techniques enabled to obtain the optimal electrical response in the absence of drilling results (DeGroot-Hedlin and Constable, 2004).

As clearly shown in Figs. 18 and 20, substantial differences, between the smooth and sharp results, are observed in the main formations. However, while the location of the primary reservoir under profile A has been identified with reasonable accuracy, in terms of electrical resistivity, its shape and geometry have not been adequately recovered. In the profile, the shape of the intrusive mass is not adequately recovered in the smooth inversion, but it is depicted more accurately in the sharp boundary inversion. Additionally, the location of the geothermal reservoir beneath profile B is quite accurate, although its geometry has not been precisely recovered; nevertheless, it aligns well with previous geological findings. From the discussed comparison, it can be inferred that the sharp boundary inversion effectively addresses the limitations of smooth inversion, particularly in high resistivity contrast zones.

As presented in Fig. 21a, the intrusive igneous body under profile A, belonging to the Eocene era, was not adequately recovered in the smoothly inverted model. By contrast, in the sharp boundary inversion (assuming a sharp resistivity gradient on the geothermal reservoir), a desirable vision of the intrusive body and heat source of the geothermal system can be obtained.

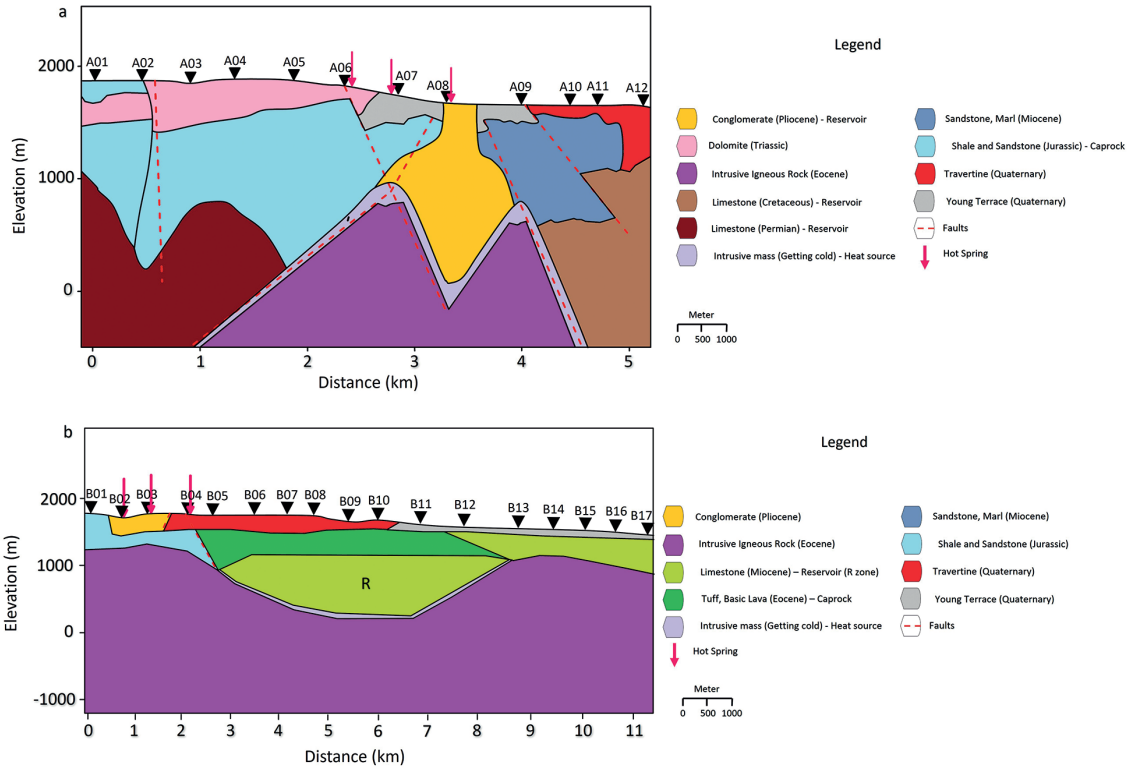

Fig. 21 - A plausible geological model based on the inverted models and geological information over Mahallat geothermal field profile A (a), and profile B (b).

The mentioned intrusive zone has been cooling down since the Eocene era and now plays a vital role as heat source. Shale and sandstone, belonging to the Jurassic era, are interpreted as impermeable cap rock in the geothermal system. The Permian limestone on the left side, Pliocene limestone on top, and Cretaceous limestone on the right side of the intrusive bodies are plausible geothermal reservoirs and consist of hydrothermal circulations. Numerous faults, evidently, lead the hydrothermal fluids to the surface where they give origin to hot springs. The location of the heat source, geothermal reservoir, faults, and hot springs illustrate a reasonable scenario of the geothermal system beneath profile A. Reaching upwards near the surface, worthy of note is that an evident fault at stations A02 and A03 caused water circulation in the Permian limestone reservoir, and that the conductivity impacts have been properly recovered within the smooth and sharp boundary inversions.

In Fig. 21b, the shallow conductive layer is attributed to young sediments and alluvial layers with a maximum depth of 500 m. Interpreted as cap rocks, underneath the conductive layer lies a semi-resistive zone consisting of Eocene tuff and basic lava (as per geological maps). The Miocene limestone reservoir charges hydrothermal circulations through the conductive zone under the impermeable cap rock. The reservoir has a depth interval ranging from -600 to -1,700 m (from the surface) and a length of 6,000 m. As can be observed, the faults cause the hydrothermal fluids to reach the Earth's surface. The Eocene intrusive body, beneath the reservoir, serves as a heat source for the geothermal reservoir.

6. Conclusions

In terms of geothermal systems, the Mahallat region is one of the high-potential zones located in central Iran. Hot springs are representative of the developed geothermal system underneath the surface. This study took advantage of the MT method to determine the geothermal field properties and distinguish the tectonics and geological features of the area. Two MT data inversion methods were examined to build a model with the best data fit and resolution. The results from both methods provide accurate information on subsurface structures. Although the inverted models facilitate the interpretation of geological conditions and resemble resistivity distribution (the essential physical features of geothermal systems), some inversion methods, under specific circumstances, may yield results that significantly diverge from the realistic situation. For instance, in the current study, the 2D smooth inversion method bears a number of constraints in which the approach may present unrealistic outcomes in the high resistivity gradient mediums. Since the geothermal fields consist of a combination of highly resistive and conductive units, in order to resolve the aforementioned issue, the 2D sharp boundary inversion method was exploited to achieve more dependable results. The properties of the 2D sharp boundary inversion method were initially evaluated on a distinct synthetic model to review and compare the differences and applicability in revealing the components of a geothermal system. Both methods were applied to properly recover the detail structures of the models, consisting of sharp gradient layers. Next, the dimensionality of the field data was determined as a 2D structure. Forasmuch as the geoelectrical strike of the study region is within the azimuth of almost zero, the TE- and TM-mode data show their actual values (no rotation).

Observing the 2D sharp boundary inversion outcome corresponding to profile A reveals the following. 1) The inverted model shows a high-resistive zone at the bottom of the section, likely representing the basement layer. Due to the resistivity disparity between basement rock (very high resistivity zones) and adjacent layers, the layer has been revealed by sharp boundary inversion in comparison to the smooth one. 2) The resistivity ranges, which are representative of geothermal components, are well recovered in terms of shape, geometry, and expansion. As illustrated, three main geothermal reservoirs, jointly related to the main faults, were identified underneath profile A. 3) The conductive cap and cap rock have also been recovered by sharp boundary algorithm as the last typical geothermal structure.

Likewise, the profile B results reveal the following. a) A highly resistive basement layer with an approximate thickness of 2,000 m. b) The identification of a relatively high-conductive zone in the middle of the inversion section (10-30 Ωm), interpreted as a geothermal reservoir. This reservoir is aligned with findings from previous studies with regards to shape and geometry (Oskooi *et al*., 2016). However, the sharp boundary algorithm refines the layering and clearly delineates the reservoir boundary. c) Ultimately, the cap rock and shallow conductive layers were classically recovered in profile B. The resistivity of the cap rocks, within this profile, varies between 500 and 200 Ωm and that of the conductive rocks varies from 5 to 40 Ωm.

Regarding the inverted models obtained using both methods, this study proposed conceptual geological models on each profile. The plausible model is obtained by composing the MT results and detailed geological facts. According to the geological sections, the following information is provided. i) Three geothermal reservoirs were specified beneath profile A; the first reservoir mainly consists of conglomerates ranging between 0 and 1,800 m. The remaining reservoirs correspond to Cretaceous and Permian limestone at an elevation of -200 to 1,200 m, affected by faults controlling the flow of the geothermal fluids within the system. ii) The remarkable capability of the 2D sharp boundary inversion is prominently evident along profile B, and more

particularly in areas with a pronounced contrast between the geothermal reservoir and intrusive igneous rocks. Geological section B illustrates the Miocene geothermal reservoir at a depth from 200 to 2,000 m. This reservoir is faulted, and, therefore, it can also control the geothermal water circulation. The deep hot water penetrates upwards through the faulted and fractured formations to, then, emerge as hot springs within the Mahallat area.

Acknowledgments. This work was originally funded by the research council of the University of Tehran (UT), Iran. The authors thank the Department of Geomagnetism of the Institute of Geophysics of UT for supplying the geophysical data. The second author (BO) acknowledges funding from the UT under the mission commandment no.: 155/1402/13713 dated 8 April 2023 for a one-year sabbatical leave starting from 21 February 2023 at the Luleå University of Technology in Sweden.

REFERENCES

Aghanabati A.; 2004: *Geology of Iran*. Geological Survey of Iran, Tehran, Iran, 361 pp., in Iranian.

Alavi M.; 1994: *Tectonics of the Zagros orogenic belt of Iran: new data and interpretations.* Tectonophys., 229, 211-238.

Araghi F.M.; 2009: *Study of Mahallat Fault using CRP method.* PH.D. Thesis in Physical Sciences, Arak University, Arak, Iran, in Farsi.

Ardestani V.E., Fournier D. and Oldenburg D.W.; 2021: *Gravity and magnetic processing and inversion over the Mahallat geothermal system using open-source resources in Python.* Pure Appl. Geophys., 178, 2171-2190.

Berberian M.; 1981: *Active faulting and tectonics of Iran.* In: Zagros Hindu Kush Himalaya Geodynamic Evolution, Gupta H.K. and Delany F.M. (eds), vol. 3, pp. 33-69, doi: 10.1029/GD003p0033.

Bostick F.X. Jr.; 1977: *A simple almost exact method of MT analysis.* In: Abstract Workshop on Electrical Methods in Geothermal Exploration, Snowbird, UT, USA, pp. 175-177.

Caldwell T.G., Bibby H.M. and Brown C.; 2004: *The magnetotelluric phase tensor.* Geophys. J. Int., 158, 457-469.

de Groot-Hedlin C. and Constable S.; 2004: *Inversion of magnetotelluric data for 2D structure with sharp resistivity contrasts*. Geophys., 69, 78-86.

Gansser A.; 1955: *2. New aspects of the geology in central Iran (Iran).* In: Proc. 4th World Petroleum Congress, Rome, Italy, WPC-6018.

Ghiasi S.M., Hosseini S.H., Afshar A. and Abedi M.; 2023: *A novel magnetic interpretational perspective on Charmaleh Iron deposit through improved edge detection techniques and 3D inversion approaches.* Nat. Resour. Res., 32, 147-170.

Ghorbani M.; 2013: *A summary of geology of Iran*. In: The economic geology of Iran: mineral deposits and natural resources, pp. 45-64, doi: 10.1007/978-94-007-5625-0_2.

Ghorbani M.; 2021: *The geology of Iran: tectonic, magmatism and metamorphism*. Springer International Publishing, Cham, Switzerland, 441 pp.

Hassanzadeh J. and Wernicke B.P.; 2016: *The Neotethyan Sanandaj-Sirjan zone of Iran as an archetype for passive margin-arc transitions*. Tectonics, 35, 586-621.

Hosseini S.H., Habibian Dehkordi B., Abedi M. and Oskooi B.; 2021: *Implications for a geothermal reservoir at Abgarm, Mahallat, Iran: magnetic and magnetotelluric signatures.* Nat. Resour. Res., 30, 259-272.

Jackson J., Priestley K., Allen M. and Berberian M.; 2002: *Active tectonics of the South Caspian Basin.* Geophys. J. Int., 148, 214-245.

Li M., Li G.M., Yang L., Dang X.Y., Zhao C.H., Hou G.C. and Zhang M.S.; 2007: *Numerical modelling of geothermal groundwater flow in karst aquifer system in eastern Weibei, Shaanxi Province, China.* Science in China Series D: Earth Sciences, 50, 36-41, doi: 10.1007/s11430-007-5020-7.

Li S., Wen D., Feng B., Li F., Yue D., Zhang Q., Wang J. and Feng Z.; 2023: *Numerical optimization of geothermal energy extraction from deep karst reservoir in north China.* Renewable Energy, 202, 1071-1085, doi: 10.1016/j.renene.2022.12.016.

McGary R.S., Evans R.L., Wannamaker P.E., Elsenbeck J. and Rondenay S.; 2014: *Pathway from subducting slab to surface for melt and fluids beneath Mount Rainier.* Nat., 511(7509), 338-340, doi: 10.1038/nature13493.

McKenzie D.S.; 1972: *Active tectonics of the Mediterranean region.* Geophys. J. R. Astron. Soc., 30, 109-185.

Mohammadzadeh-Moghaddam M., Oskooi B., Mirzaei M. and Jouneghani S.J.; 2012: *Magnetic studies for geothermal exploration in Mahallat, Iran.* In: Proc. International Geophysical Conference and Oil & Gas Exhibition, Society of Exploration Geophysicists and The Chamber of Geophysical Engineers of Turkey, Istanbul, Turkey, 4 pp., doi: 10.1190/IST092012-001.62.

Munoz G.; 2014: *Exploring for geothermal resources with electromagnetic methods.* Surv. Geophys., 35, 101-122.

Muñoz G., Ritter O. and Moeck I.; 2010: *A target-oriented magnetotelluric inversion approach for characterizing the low enthalpy Groß Schönebeck geothermal reservoir.* Geophys. J. Int., 183, 1199-1215.

Najafi G. and Ghobadian B.; 2011: *Geothermal resources in Iran: the sustainable future.* Renewable Sustainable Energy Rev., 15, 3946-3951.

Navai I.; 1976: *Activities of the Geological Survey of Iran in remote sensing.* In: Proc. CENTO Workshop on Applications of Remote Sensing Data and Methods, Istanbul, Turkey, U.S. Geological Survey, Reston, VA, USA, pp. 135-136.

Niblett E.R. and Sayn-Wittgenstein C.; 1960: *Variation of electrical conductivity with depth by the magneto-telluric method.* Geophys., 25, 998-1008.

Noorollahi Y., Yousefi H., Itoi R. and Ehara S.; 2009: *Geothermal energy resources and development in Iran.* Renewable Sustainable Energy Rev., 13, 1127-1132.

Noorollahi Y., Shabbir M.S., Siddiqi A.F., Ilyashenko L.K. and Ahmadi E.; 2019: *Review of two decade geothermal energy development in Iran, benefits, challenges, and future policy.* Geotherm., 77, 257-266.

Nouraliee J., Porkhial S., Mohammadzadeh-Moghaddam M., Mirzaei S., Ebrahimi D. and Rahmani M.R.; 2015: *Investigation of density contrasts and geologic structures of hot springs in the Markazi Province of Iran using the gravity method.* Russ. Geol. Geophys., 56, 1791-1800.

Oskooi B. and Ansari S.M.; 2012: *Application of magnetotelluric method in exploration of geothermal reservoirs with an example from Iceland.* J. Earth Space Phys., 37, 93-106, doi: 10.22059/JESPHYS.2012.24304.

Oskooi B. and Darijani M.; 2014: *2D inversion of the magnetotelluric data from Mahallat geothermal field in Iran using finite element approach.* Arabian J. Geosci., 7, 2749-2759.

Oskooi B., Darijani M. and Mirzaei M.; 2013: *Investigation of the electrical resistivity and geological structures on the hot springs in Markazi province of Iran using magnetotelluric method.* Boll. Geof. Teor. Appl., 54, 245-256, doi: 10.4430/bgta0102.

Oskooi B., Mirzaei M., Mohammadi B., Mohammadzadeh-Moghaddam M. and Ghadimi F.; 2016: *Integrated interpretation of the magnetotelluric and magnetic data from Mahallat geothermal field, Iran.* Stud. Geophys. Geod., 60, 141-161.

Peng C., Pan B., Xue L. and Liu H.; 2019: *Geophysical survey of geothermal energy potential in the Liaoji Belt, northeastern China.* Geotherm. Energy, 7, 14, 19 pp., doi: 10.1186/s40517-019-0130-y.

Porkhial S., Nouraliee J., Rahmani M. and Ebrahimi D.; 2013: *Resource assessment of Vartun geothermal region, central Iran.* J. Tethys, 1, 29-40.

Ritz J.F., Nazari H., Salamati R., Shafeii A., Solaymani S. and Vernant P.; 2006: *Active transtension inside central Alborz: a new insight into the northern Iran - southern Caspian geodynamics.* Geol., 34, 477-480.

Rodi W. and Mackie R.L.; 2001: *Nonlinear conjugate gradients algorithm for 2-D magnetotelluric inversion.* Geophys., 66, 174-187.

Sarvandani M.M., Kalateh A.N., Unsworth M. and Majidi A.; 2017; *Interpretation of magnetotelluric data from the Gachsaran oil field using sharp boundary inversion.* J. Pet. Sci. Eng., 149, 25-39.

Shirani S., Kalateh A.N. and Mohammadzadeh-Moghaddam M.; 2020; *Estimation of geothermal parameters using spectral analysis and 3D inverse modelling of the magnetic data in the Mahallat geothermal field.* Adv. Appl. Geol., 10, 328-353, doi: 10.22055/AAG.2020.28917.1957.

Singarimbun A., Gaffar E.Z. and Tofani P.; 2017: *Modeling of reservoir structure by using magnetotelluric method in the area of Mt. Argopuro, east Java, Indonesia.* J. Eng. Technol. Sci., 49, 833-847, doi: 10.5614/j.eng.technol.sci.2017.49.6.9.

Smith J.T. and Booker J.R.; 1988: *Magnetotelluric inversion for minimum structure.* Geophys., 53, 1565-1576.

Smith T., Hoversten M., Gasperikova E. and Morrison F.; 1999: *Sharp boundary inversion of 2D magnetotelluric data.* Geophys. Prospect., 47, 469-486.

SUNA; 1998: *Country Geothermal Potential Survey*. Renewable Energies Office, Ministry of Energy, Tehran, Iran, 1st Phase Report, 306 pp.

Talebi M.A., Hosseini S.H., Abedi M. and Moradzadeh A.; 2023: *3D inverse modelling of electrical resistivity and chargeability data through unstructured meshing, a case study for travertine exploration.* Int. J. Min. Geo-Eng., 57, 131-140. doi: 10.22059/ijmge.2022.347290.594991.

Tian J., Pang Z., Liao D. and Zhou X.; 2021: *Fluid geochemistry and its implications on the role of deep faults in the genesis of high temperature systems in the eastern edge of the Qinghai Tibet Plateau.* Appl. Geochem., 131, 105036, doi: 10.1016/j.apgeochem.2021.105036.

Tikhonov A.N. and Arsenin V.; 1977: *Solutions of ill-posed problems*. Winston & Sons, Washington, DC, USA, 258 pp., translated from Russian.

Vozoff K.; 1972: *The magnetotelluric method in the exploration of sedimentary basins.* Geophys., 37, 98-141.

Yazdi M., Hassanvand M., Tamasian O. and Navi P.; 2016: *Hydrogeochemical characteristics of Mahallat hot springs, central Iran.* J. Tethys, 4, 169-179.

Yousefi H., Noorollahi Y., Ehara S., Itoi R., Yousefi A., Fujimitsu Y. and Sasaki K.; 2010: *Developing the geothermal resources map of Iran.* Geotherm., 39, 140-151.

Corresponding author: Behrooz Oskooi
Institute of Geophysics, University of Tehran
Kargar Shomali, Tehran, Iran
Phone: + 98 21 6111 8238; e-mail: boskooi@ut.ac.ir